IEEE Access
Multidisciplinary : Rapid Review : Open Access Journal

Received October 26, 2020, accepted November 6, 2020, date of publication November 24, 2020, date of current version December 9, 2020.

Digital Object Identifier 10.1109/ACCESS.2020.3040177

A Logistic Chaotic Barnacles Mating Optimizer With Masi Entropy for Color Image Multilevel Thresholding Segmentation

HONGBO LI[1], GANG ZHENG[1], KANGJIAN SUN[1], ZICHAO JIANG[1], YAO LI[1], AND HEMING JIA[2], (Member, IEEE)
[1]College of Mechanical and Electrical Engineering, Northeast Forestry University, Harbin 150040, China
[2]College of Information Engineering, Sanming University, Sanming 365004, China

Corresponding author: Gang Zheng (ericzg@nefu.edu.cn)

This work was supported by the Fundamental Research Funds for the Central Universities under Grant 2572018BF10.

ABSTRACT Barnacles mating optimizer (BMO) is an evolutionary algorithm that simulates the mating and reproductive behavior of barnacle population. In this article, an improved Barnacles mating optimizer based on logistic model and chaotic map (LCBMO) was proposed to produce the high-quality optimal result. Firstly, the logistic model is introduced into the native BMO to realize the automatic conversion parameters. This strategy maintains a proper relationship between exploitation and exploration. Then, the chaotic map is integrated to enhance the exploitation capability of the algorithm. After that, six variants based on LCBMO are compared to find the best algorithm on benchmark functions. Moreover, to the knowledge of the authors, there is no previous study on this algorithm for multilevel color image segmentation. LCBMO takes Masi entropy as the objective function to find the optimal threshold. By comparing different thresholds, different types of images, different optimization algorithms, and different objective functions, our proposed technique is reliable and promising in solving color image multilevel thresholding segmentation. Wilcoxon rank-sum test and Friedman test also prove that the simulation results are statistically significant.

INDEX TERMS Barnacles mating optimizer, logistic model, chaotic map, Masi entropy, multilevel thresholding, color image segmentation.

I. INTRODUCTION

With the emergence of computer technology, image processing has been widely used in many fields. Image segmentation is one of the classical topics in image processing [1]. It divides the original image into significative and multiple sub-regions according to intensity, color, texture and other attributes of the image [2]. Image segmentation is often the pretreatment stage of higher-class processing such as: image analysis, object recognition, and computer vision. Consequently, the performance of higher-class processing system depends on the accuracy of the segmentation technique adopted [3]. Researchers have proposed many kinds of segmentation, including edge detection, histogram based thresholding, region, feature clustering, and neural networks [4]–[6]. Histogram based thresholding is a simple and the most commonly used image segmentation approach [7], [8]. Thresholding methods can be divided into two categories: bi-level thresholding and multi-level thresholding. Bi-level thresholding means that the target and background can be clearly distinguished by a single threshold value. Multi-level thresholding denotes that the given image can be segmented into various classes by multiple threshold values [9]–[11].

In recent years, the methods to determine the optimal threshold for a given image can be divided into two categories: parametric and non-parametric methods [12]. In the parametric techniques, it is assumed that the probability density function of each class is known. The common parameter methods generally follow a certain distribution of probability density, such as Gauss distribution [13], Poisson distribution [14], [15], generalized Gaussian distribution [16], and so on. This methods differs from the actual situation to some extent. In addition, the segmentation is affected when classes

The associate editor coordinating the review of this manuscript and approving it for publication was Seyedali Mirjalili.

are highly overlapped. Therefore, the parametric approaches are not ideal choices in this case. For non-parametric methods, the probability density function is usually unknown, and the threshold is generally searched by optimizing the objective function [17]. The classical non-parametric methods are mainly as follows: Otsu proposed a method to maximize the variance between classes at first [18]. Then the methods based on information entropy theory are proposed, which are categories to measure homogeneity. Among them, the most representative entropy approaches for image segmentation include: Minimum Cross entropy [19], Kapur entropy [20], Renyi entropy [21], Tsallis entropy [22], and Masi entropy [23]. They can be easily extended to multi-level thresholding.

Among them, a novel generalized entropy measurement called Masi entropy has attracted increasing attention in the past few years. Furthermore, Tsallis and Renyi entropies are two different generalizations along two different paths. Furthermore, Tsallis entropy is generalized to non-extensive systems, while Renyi entropy is quasi-linear devices. However, Masi entropy is extended to non-extensive systems and non-linear devices, including Tsallis entropy and Renyi entropy [24], [25]. A publication for multilevel thresholding segmentation of color satellite images based on Masi entropy has been proposed by Shubham in 2019. Simulation results show that the proposed method is effective and has better segmentation performance than Kapur, Renyi and Tsallis entropy [26]. Although the exhaustive search is effective in image segmentation, it cannot find the optimal threshold, and the complexity increases exponentially with the number of thresholds. [27], [28]. In order to speed up this process, one option is to replace some classical exhaustive searches based on meta-heuristic search algorithms.

Sulaiman proposed a novel bio-inspired algorithm called Barnacles mating optimizer (BMO) in 2020 [29]. Obviously, the BMO algorithm simulates the intelligent behavior of barnacles in nature, including selection process and reproduction. It can be seen from the lecture that the BMO algorithm has outstanding convergence ability, fast convergence speed and excellent search ability. But according to the no free lunch theorem, it can be seen that no independent algorithm can solve all optimization problems [30]. Therefore, the BMO algorithm need to be improved. The logistic regression model is a common improvement strategy and widely used in various optimization methods. In 2018, Qasim *et al.* applied logistic regression model for optimization of feature selection. The results showed that the proposed method can obtain a great classification performance with few features [31]. In 2019, by using logistic regression prediction model, Ghazvini *et al.* solved the problem of the variables affecting tuberculosis [32]. Therefore, this article chooses logistic regression model to improve BMO. Meanwhile, chaotic map is an excellent mathematical strategies, which can improve the performance of meta-heuristic algorithm in avoiding local optimization. Chaotic map can provide random behavior without random component [33]. Accordingly, scholars have added chaotic map to the

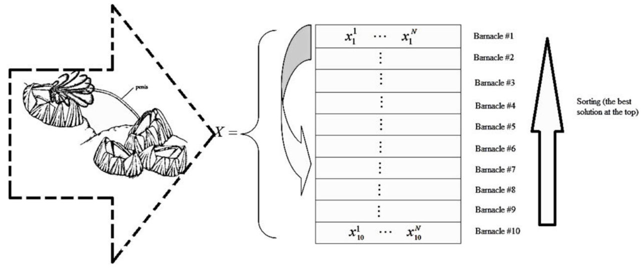

FIGURE 1. Selection of mating process of ten barnacles [69].

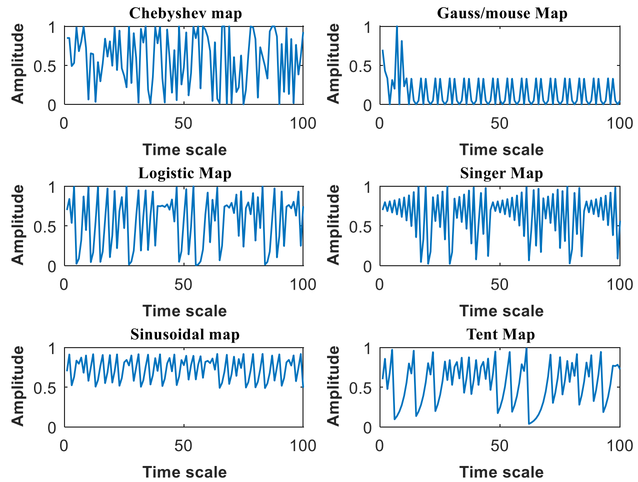

FIGURE 2. Visualization of six different chaotic maps.

optimization algorithm to improve the ability of algorithms. J. Alikhani Koupaei *et al.* proposed a new optimization algorithm based on chaotic maps. Experimental results proved that the modified algorithm was competitive in multi/unimodal objective functions [34]. A. Naanaa embedded spatiotemporal map into chaos optimization algorithms to improve its convergence and efficiency [35]. Yang *et al.* proposed chaos optimization algorithms based on chaotic maps to achieve the high efficiency, which improve the convergence speed and accuracy [36]. Chuang *et al.* combined chaotic maps with s binary particle swarm optimization, which sped up search process the algorithm [37]. Motivated by these successful applications of the strategies, the authors introduce logistic model and chaotic map into BMO algorithm to increase the diversity of algorithm and prevent skipping over the optimal solutions. In addition, it also better balances the exploration and exploitation trends.

Image segmentation based on histogram and global threshold is most commonly used to determine threshold value. Masi entropy is a bi-level threshold method based on the gray level and its histogram. And Masi entropy objective functions can be maximized by LCBMO to find the optimum threshold value. Furthermore, the provided image is segmented into unique classes. In this article, a series of experiments are conducted, and the experimental results are analyzed and discussed in details. The performance of image segmentation is measured in terms of objective function values, peak

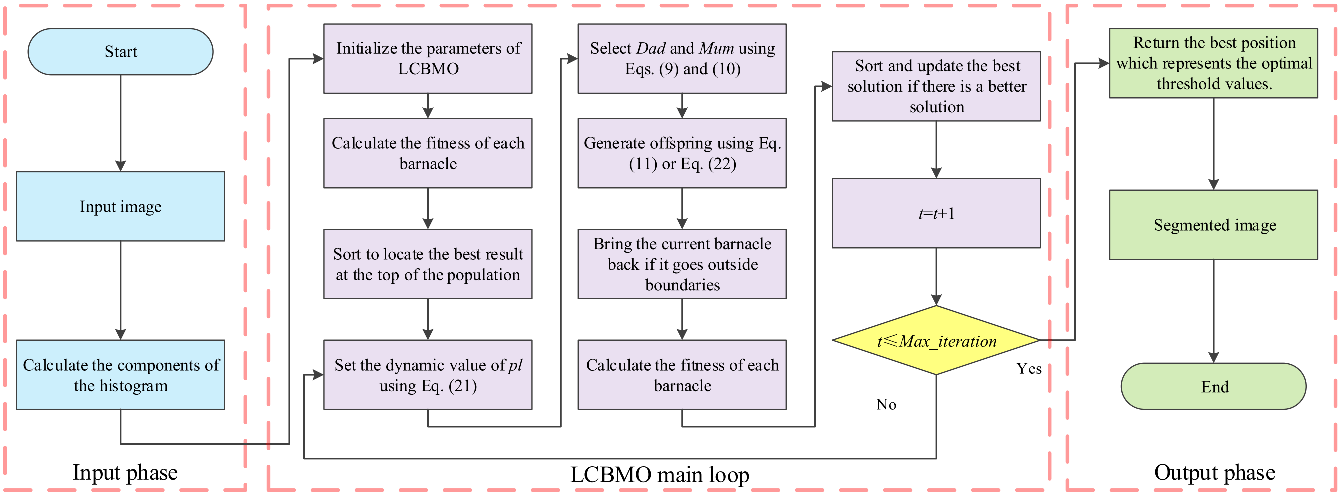

FIGURE 3. Flowchart of the LCBMO algorithm based multilevel thresholding method.

signal-to-noise ratio (PSNR) [38], [39], structural similarity index (SSIM) [40]–[42], feature similarity (FSIM) [43], [44], Wilcoxon rank-sum test [45], [46], and Friedman test [47]. In order to compare various algorithms more intuitively, the convergence curve based on objective function values are drawn. The experimental results confirm that the proposed Barnacles mating optimizer based on logistic model and chaotic map can be effectively used for multilevel thresholding.

The remainder of this article is organized as follows: Section II discusses related studies. Section III outlines some preliminaries. Section IV gives the proposed BMO based on logistic model and chaotic map for multilevel thresholding color image segmentation. The benchmark functions experiments are presented in Section V. Other simulation experiments and results analysis are described in Section VI. Finally, Section VII concludes the work and suggests some directions for future studies.

II. LITERATURE REVIEW

In 2015, A.K. Bhandari *et al.* proposed satellite image segmentation model based on modified artificial bee colony algorithm, in which the Kapur, Tsallis and Otsu functions are used to determine the threshold [48]. And in 2016, Mozaffari *et al.* introduced an inclined planes system optimization algorithm to solve the problems in different fields of science and engineering [49]. The convergence heterogeneous particle swarm was utilized to find the best thresholds in literature, which has the better stability and convergence in 2017 [50]. Oliva *et al.* combines cross entropy with crow search algorithm for image segmentation to reduce computational complexity in the same year [51]. H. N. Liang *et al.* applied modified grasshopper algorithm in image segmentation technology, which showed excellent results [52]. Furthermore, cuckoo search algorithm based on minimum cross entropy is proposed to make the method more practical and uncomplicated [53]. In 2018, S. Kotte presented an improved differential search algorithm for gray scale images to increase its computational efficiency and accuracy of segmentation [54]. In 2019, H. S. Gill exploits minimize cross entropy as the objective function, and uses teaching-learning-based optimization algorithm to select multilevel threshold values. The experimental outcomes indicate the proposed method has an advantage of efficiency and robustness [55]. S. J. Mousavirad published the human mental to search the optimal threshold to increase segmentation efficiency [56]. Bohat studied a new heuristic for multilevel thresholding of images, and combined whale optimization algorithm. Meanwhile, the results demonstrate that the proposed algorithm is superior to the other algorithm [57]. A novel beta differential evolution algorithm-based fast multilevel thresholding is applied for color image segmentation in 2020. Then the performance is proved to be superior to other methods in image segmentation such as artificial bee colony, particle swarm optimization and differential evolution [58]. And a competitive swarm algorithm was applied in image segmentation guided based opposite fuzzy entropy to improve the segmentation accuracy in the same year [59]. Furthermore, a benchmark of recent population-based metaheuristic algorithms was proposed for high-dimensional multi-level maximum variance threshold selection, which has attract much attention [60]. D. Oliva combined the thresholding techniques and the evolutionary Bayesian network algorithm to generate the accurate class even in complex condition [61]. E. R. Esparza represented an efficient harris hawks method used into the image segmentation so as to produce the efficient and reliable results [62].

These algorithms are successfully applied to multilevel thresholding and reduce the computational complexity, which inspire further research by scholars.

III. MATERIAL AND METHODS

A. MULTILEVEL THRESHOLDING

Threshold segmentation processes the digital image histogram. We use an algorithm as the segmentation

TABLE 1. Results of benchmark functions.

Function		BMO	LCBMO-1	LCBMO-2	LCBMO-3	LCBMO-4	LCBMO-5	LCBMO-6
F1	Mean	2.7456E-104	8.0670E-122	**2.0982E-138**	4.9079E-132	3.0311E-131	3.4664E-128	2.5972E-131
	Std	1.5036E-103	4.2272E-121	**1.1492E-137**	2.4220E-131	1.5751E-130	1.8982E-127	1.0009E-130
F2	Mean	1.3881E-54	2.2668E-62	**5.5896E-73**	1.1049E-67	1.1786E-64	7.1625E-67	2.5444E-67
	Std	6.2307E-54	6.7554E-62	**1.8738E-72**	4.6165E-67	6.2120E-64	3.7995E-66	9.9918E-67
F3	Mean	3.4180E-102	5.1183E-122	5.3994E-126	4.1877E-132	4.0884E-131	1.3896E-128	**7.9177E-141**
	Std	1.3858E-101	2.7389E-121	2.9574E-125	1.9593E-131	1.6927E-130	7.6110E-128	**4.2957E-140**
F4	Mean	3.6797E-50	2.0731E-60	**3.5046E-71**	9.3413E-67	4.9115E-68	6.3592E-68	3.1208E-68
	Std	2.0154E-49	1.1008E-59	**1.8882E-70**	4.6508E-66	2.6334E-67	2.3039E-67	1.3970E-67
F5	Mean	**2.8608E+01**	2.8708E+01	2.8697E+01	2.8634E+01	2.8659E+01	2.8661E+01	2.8666E+01
	Std	1.3377E-01	**1.0713E-01**	1.3578E-01	1.2642E-01	1.2173E-01	1.7660E-01	1.1627E-01
F6	Mean	3.2407E+00	3.3267E+00	**2.9480E+00**	3.4678E+00	3.3950E+00	3.4415E+00	3.5499E+00
	Std	4.4858E-01	4.8817E-01	**3.7241E-01**	5.2348E-01	5.0161E-01	4.5087E-01	3.7263E-01
F7	Mean	2.4745E-04	**1.5032E-04**	1.7646E-04	1.6915E-04	1.7598E-04	2.3721E-04	1.6801E-04
	Std	2.1311E-04	2.0998E-04	2.3254E-04	2.0896E-04	1.7959E-04	2.3736E-04	**1.5103E-04**
F8	Mean	-5.7997E+03	-4.0807E+03	-3.9814E+03	**-4.1040E+03**	-3.8691E+03	-3.9180E+03	-3.8819E+03
	Std	**6.9936E+02**	1.0228E+03	9.4000E+02	9.4871E+02	8.0760E+02	9.9503E+02	9.3137E+02
F9	Mean	**0.0000E+00**	**0.0000E+00**	**0.0000E+00**	**0.0000E+00**	**0.0000E+00**	**0.0000E+00**	**0.0000E+00**
	Std	**0.0000E+00**	**0.0000E+00**	**0.0000E+00**	**0.0000E+00**	**0.0000E+00**	**0.0000E+00**	**0.0000E+00**
F10	Mean	**8.8818E-16**	**8.8818E-16**	**8.8818E-16**	**8.8818E-16**	**8.8818E-16**	**8.8818E-16**	**8.8818E-16**
	Std	**0.0000E+00**	**0.0000E+00**	**0.0000E+00**	**0.0000E+00**	**0.0000E+00**	**0.0000E+00**	**0.0000E+00**
F11	Mean	**0.0000E+00**	**0.0000E+00**	**0.0000E+00**	**0.0000E+00**	**0.0000E+00**	**0.0000E+00**	**0.0000E+00**
	Std	**0.0000E+00**	**0.0000E+00**	**0.0000E+00**	**0.0000E+00**	**0.0000E+00**	**0.0000E+00**	**0.0000E+00**
F12	Mean	2.7451E-01	3.2043E-01	**1.8922E-01**	2.8045E-01	3.4166E-01	2.9491E-01	3.4588E-01
	Std	**1.0270E-01**	8.6751E-02	5.9385E-02	8.3200E-02	1.3080E-01	7.9854E-02	1.2573E-01
F13	Mean	2.9798E+00	2.9779E+00	**2.9784E+00**	2.9818E+00	2.9818E+00	2.9819E+00	2.9821E+00
	Std	**1.5409E-03**	2.0415E-02	1.9976E-02	2.4983E-03	1.5493E-03	1.8747E-03	2.0256E-03
F14	Mean	**9.9830E+00**	1.0694E+01	9.2442E+00	1.1119E+01	8.5327E+00	9.5436E+00	1.0316E+01
	Std	3.6994E+00	**2.8149E+00**	3.8806E+00	2.9583E+00	3.8008E+00	4.3413E+00	3.7889E+00
F15	Mean	5.9055E-04	5.3476E-04	5.4436E-04	5.1764E-04	**5.1406E-04**	6.6665E-04	5.7058E-04
	Std	7.9877E-04	3.9538E-04	4.8363E-04	**2.9702E-04**	3.3917E-04	6.4106E-04	4.3494E-04
F16	Mean	-1.0316E+00	-1.0316E+00	-1.0312E+00	-1.0313E+00	-1.0316E+00	-1.0316E+00	-1.0316E+00
	Std	**1.1726E-10**	3.0155E-08	2.0588E-03	8.1873E-04	2.0418E-09	2.7294E-08	1.2335E-05
F17	Mean	**3.9789E-01**	**3.9789E-01**	**3.9789E-01**	**3.9789E-01**	**3.9789E-01**	**3.9789E-01**	**3.9789E-01**
	Std	6.8631E-06	3.8505E-07	8.2335E-08	**5.0036E-09**	1.8101E-07	8.1594E-08	8.0256E-08
F18	Mean	3.0001E+00	**3.0000E+00**	3.9946E+00	3.3127E+00	3.6133E+00	3.0483E+00	4.0239E+00
	Std	3.3832E-04	**8.8141E-06**	4.9389E+00	1.7119E+00	3.3436E+00	2.0203E-01	4.9463E+00
F19	Mean	**-3.0048E-01**	**-3.0048E-01**	**-3.0048E-01**	**-3.0048E-01**	**-3.0048E-01**	**-3.0048E-01**	**-3.0048E-01**
	Std	**0.0000E+00**	**0.0000E+00**	**0.0000E+00**	**0.0000E+00**	**0.0000E+00**	**0.0000E+00**	**0.0000E+00**
F20	Mean	-3.2940E+00	-3.2846E+00	**-3.2946E+00**	-3.2588E+00	-3.2868E+00	-3.2598E+00	-3.2507E+00
	Std	6.3265E-02	5.9113E-02	**4.7664E-02**	1.6016E-01	9.1560E-02	1.3013E-01	1.1327E-01
F21	Mean	-5.0762E+00	-5.0550E+00	-5.0546E+00	-5.0548E+00	-5.0068E+00	**-5.1213E+00**	-5.0545E+00
	Std	1.1538E-01	**3.1608E-04**	1.0224E-03	4.6342E-04	2.6253E-01	3.6470E-01	1.4294E-03
F22	Mean	-5.0871E+00	-5.0872E+00	-5.0873E+00	**-5.0876E+00**	-5.0689E+00	-5.0873E+00	-5.0864E+00
	Std	7.9617E-04	1.1689E-03	5.8886E-04	**6.7546E-05**	9.8831E-02	6.7017E-04	3.6973E-03
F23	Mean	-5.1283E+00	-5.1280E+00	**-5.3087E+00**	-5.1278E+00	-5.1279E+00	-5.1278E+00	-5.1373E+00
	Std	**2.3597E-04**	8.3436E-04	9.8735E-01	1.2471E-03	1.3436E-03	1.4594E-03	5.0919E-02

criterion, and the threshold that satisfies the criterion function is called the optimal segmentation threshold. By comparing with the optimal threshold, the image is divided into target region and background region. The image threshold method can be summarized into two categories: bi-level thresholding segmentation and multilevel thresholding segmentation. Bi-level thresholding segmentation cannot completely extract the target at a particular image segmentation, so we need multilevel thresholding to divide the whole image into multiple regions. Multilevel thresholding segmentation can highlight the features among image regions.

For a n-bit gray image, the gray level of the image is $L = 2^n$ and the gray level interval is $\{0, 1, \ldots, L-1\}$. n_i denotes the number of pixels whose gray level is i. N denotes the total number of pixels. p_i denotes the probability density of ith the gray value. They are defined as follows:

$$N = \sum_{i=0}^{L-0} n_i \tag{1}$$

$$p_i = \frac{n_i}{N} \tag{2}$$

$$\sum_{i=0}^{L-0} p_i = 1 \tag{3}$$

Suppose there are K thresholds of $t_1, t_2, \ldots, t_k$. They divide the gray level of a given image into K + 1 classes:

$$\begin{aligned} C_0 &= [0, 1, \ldots, t_1] \\ C_1 &= [t_1+1, t_1+2, \ldots, t_2] \\ C_k &= [t_k+1, t_k+2, \ldots, L-1] \end{aligned}$$

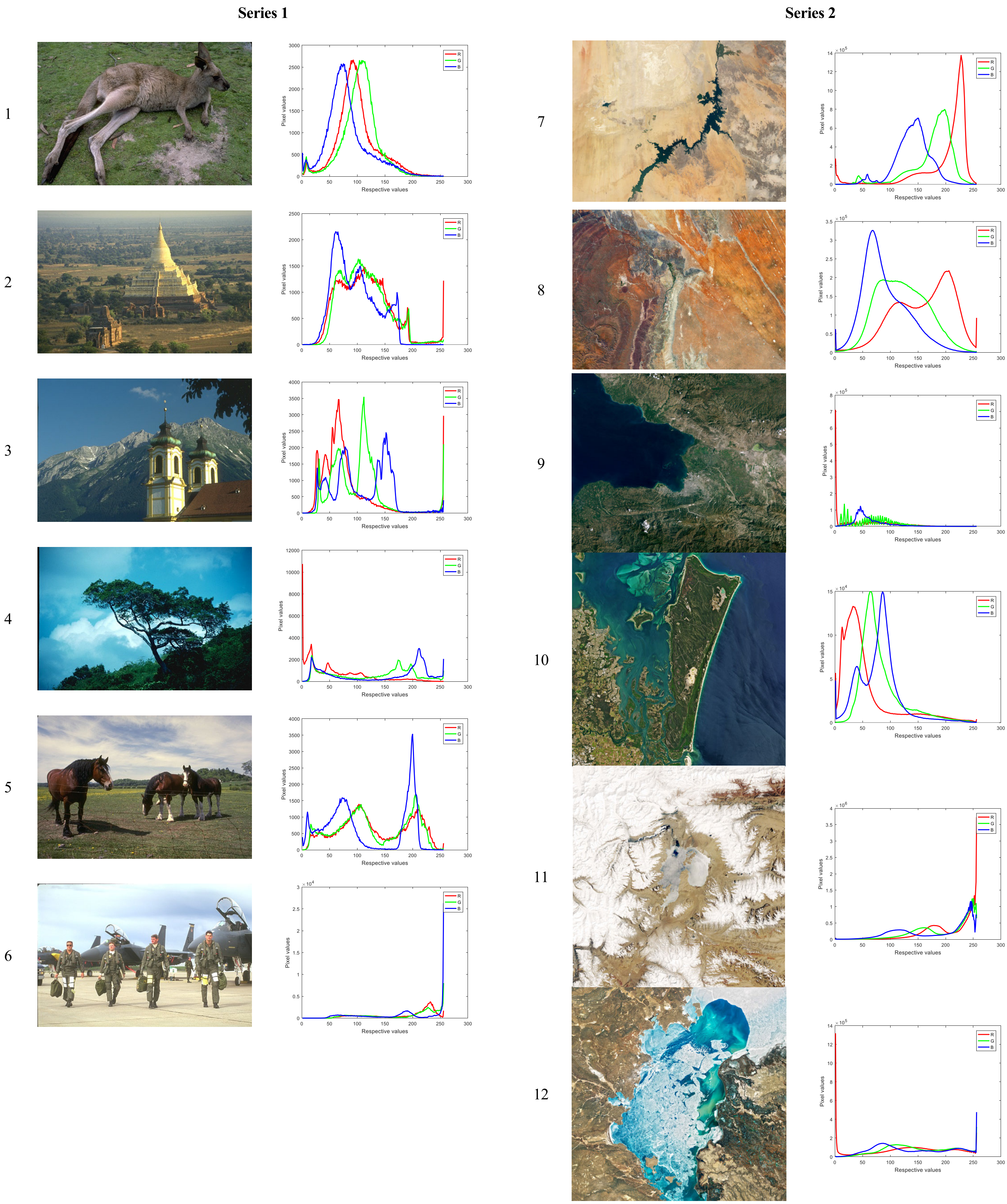

FIGURE 4. **Original test images and histograms of color channels.**

The selection of threshold is very critical, and it is related to the quality of the segmentation results. In this article, Masi entropy method are adopted.

B. MASI ENTROPY

According to Tsallis and Renyi entropy, Masi proposed a novel generalized entropic measure by introducing the

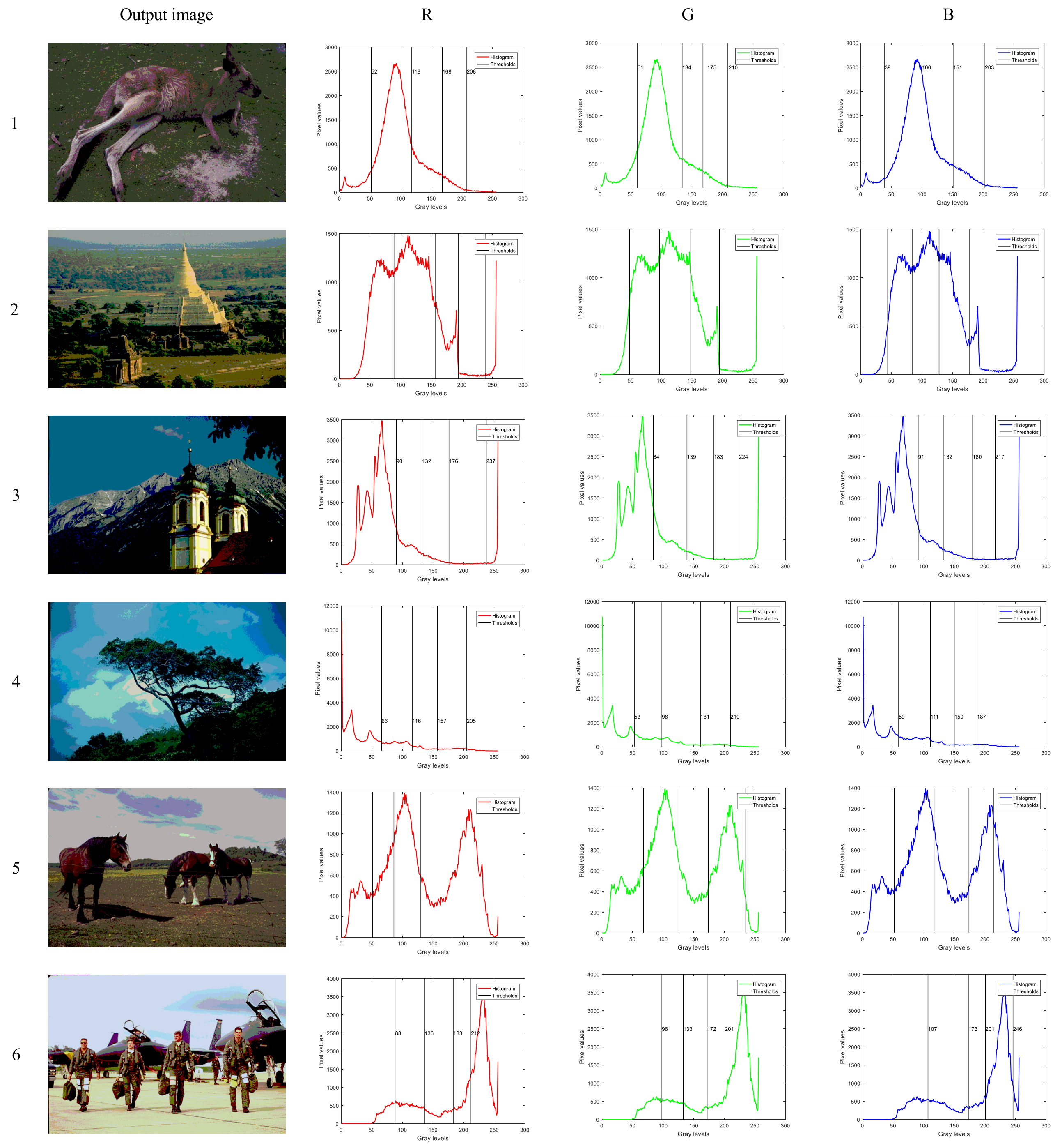

FIGURE 5. The segmentation results based on LCBMO-2 algorithm at K = 4.

concept of conventional thermodynamic entropies in 2005 [23]. Masi entropy segment color images by utilizing thorough probability function, and its detailed definition is as follows:

$$\omega_j = \sum_{i \in C_j} Pi \tag{4}$$

Eq. (4) is proposed to express the probabilities of class occurrence $\omega_j, 0 \leq j \leq k$. Based on the non-extensivity of Tsallis entropy the additivity of Renyi entropy, Eqs. (5) and (6) for calculating Masi entropy are proposed, where E_j stands for Masi entropy. $r \leq 0, r \neq 1$, In this article, the power parameter r is set to 1.18 through experiments [24].

$$E_j = \frac{1}{1-r} \log \left[1 - (1-r) \sum_{i \in C_j} \left(\frac{Pi}{\omega_j} \right) \log \left(\frac{Pi}{\omega_j} \right) \right] \tag{5}$$

$$\psi \left(t_1, t_2, \cdots, t_k \right) = \sum_{j=0}^{k} E_j \tag{6}$$

TABLE 2. Parameters of the compared algorithms.

Algorithm	Parameters	Value
CSA	Awareness probability AP	0.1
	Flight length f	2
	Random number r_1, r_2	[0,1]
GOA	Minimum c	0.00001
	Maximum c	1
CS	Mutation probability value P_a	0.25
	Scale factor β	1.5
TLBO	Teaching factor TF	1
	Random number r	[0,1]
EO	Parameter a_1	2
	Parameter a_2	1
	Parameter λ	[0,1]
	Generation probability GP	0.5
MPA	Parameter P	0.5
	Fish aggregating devices $FADs$	0.2
MABC	Random number r	[0,1]
IDSA	Random number r	[0,1]
WOA-TH	Parameter a	[0,2]
	Constant b	1
	Random number l	[-1,1]
	Constant a_0	13
	Initial value G_0	40
BDE	Number of objectives	1
	Number of constraints	0
	Number of decision variables	4
	Scaling factor	0.5
	Crossover probability	0.2
LCBMO	Random number p	[0,1]
	Initial decay rate λ	0.05
	Initial value of chaos map	0.7

Masi entropy method obtains the optimal threshold values according to maximizing the total entropy. The optimal threshold is represented by Eq. (7).

$$\left\{t_1^*, t_2^*, \cdots, t_k^*\right\} = \underset{0<t_1<t_2\cdots<t_k<L-1}{\arg\max} \left(\psi\left(t_1, t_2, \cdots, t_k\right)\right) \quad (7)$$

Compared with the histogram of grey scale image, the RGB image is more complex. In RGB space, every color pixel of the image is composed of red, green and blue [63], [64]. In this article, three channel components of R, G and B are extracted at first. Then, each channel is calculated by Masi entropy, and the objective function is maximized to find the optimal threshold for the corresponding channel [65]. The RGB channel components are divided by the optimal threshold and then merged to form the ultimate segmented image.

C. BARNACLES MATING OPTIMIZER

Barnacles mating optimizer (BMO) [29] is a novel bio-inspired optimization algorithm inspired by the mating process of barnacles. Barnacles live in water and are famous for their long penises [66]. According to initialization, selection, and reproduction, simulation optimization process is realized. The mathematical model is described in details as follows.

In the initialization process, the barnacle population can be expressed in the following matrix.

$$X = \begin{bmatrix} x_1^1 & \dots & x_1^n \\ \vdots & \ddots & \vdots \\ x_N^1 & \dots & x_N^n \end{bmatrix} \quad (8)$$

where N is the number of barnacle population, n is the number of control variables. In the next selection process, the parents to be mated are randomly selected from the population. The mathematical forms are proposed in Eq. (9) and (10).

$$barnacle\_d = randperm(N) \quad (9)$$

$$barnacle\_m = randperm(N) \quad (10)$$

where $barnacle\_d$ represents the *Dad* of the offspring, $barnacle\_m$ represents the *Mum* of the offspring.

In the reproduction process, BMO mainly produces the offspring based on Hardy-Weinberg principle [67], [68]. The interesting fact is that the penis length of the barnacle (pl) plays an important role in determining the exploitation and exploration of BMO algorithm. When pl is equal to 7, it can see from Fig. 1 that barnacle #1 can only mate with one of the barnacles #2-#7. Then, the exploitation process will be occurred. In this case, Eq. (11) is proposed to produce new offspring from parents.

$$x_i^{N\_new} = px_{barnacle\_d}^N + qx_{barnacle\_m}^N \quad (11)$$

where p is a random number drawn from the standard normal distribution between [0, 1], $q = (1-p)$, $x_{barnacle\_d}^N$ and $x_{barnacle\_m}^N$ are the variables of *Dad* and *Mum* of barnacles respectively which are selected in Eq. (9) and (10). Furthermore, p and q represent the percentage of genotype of *Dad* and *Mum* in the new generation. The new offspring is produced based on genotype frequencies p and q of parents. If barnacle #1 mates with barnacle #8-#10, the offspring is proceeded by sperm cast process. Then, the exploration process will be occurred. In this case, Eq. (12) is proposed to produce new offspring from parents.

$$x_i^{n\_new} = rand() \times x_{barnacle\_m}^n \quad (12)$$

where $rand()$ is the random number between [0, 1]. It can be noted that Eq. (12) shows the new offspring is produced only based on *Mum*. Generally, the positions of barnacles are updated in each iteration by Eq. (11) or Eq. (12) to find the best position (the best solution).

D. LOGISTIC MODEL

The adaptive parameter allows the algorithm to smoothly transit between exploration and exploitation. Therefore, it is important to choose a suitable conversion model. The logistic model and its mathematical expression are given as following [70]. How the conversion parameter accords with the change law of logistic model will be introduced in Section III.

$$\begin{cases} \dfrac{dP(t)}{dt} = \lambda \cdot (1 - \dfrac{P(t)}{P_{\max}}) \cdot P(t) \\ P(0) = P_{\min} \end{cases} \quad (13)$$

TABLE 3. The PSNR of each algorithm under Masi entropy.

IMAGE	K	CSA	GOA	CS	TLBO	EO	MPA	LCBMO-2
1	4	16.7737	15.1415	14.8758	16.9725	16.9849	15.9463	**17.0351**
	8	22.4884	19.8869	15.0566	23.6259	21.8374	22.7054	**24.0551**
	12	25.0843	22.3833	17.5726	26.2105	23.8129	26.2196	**27.4720**
	16	26.6106	24.9792	19.1451	29.2858	25.5035	28.6755	**29.9519**
2	4	16.1585	16.3893	10.3505	15.3004	17.7529	**18.7559**	18.0045
	8	23.0058	17.9405	11.9013	**24.7892**	21.7227	23.2093	24.7084
	12	24.3936	18.1793	12.7747	25.5095	23.9062	25.8181	**26.7896**
	16	26.9856	20.7563	20.2220	29.7386	25.7934	29.9196	**30.6855**
3	4	13.4553	13.7312	14.4236	14.4024	**17.9079**	16.7418	14.4094
	8	20.4363	16.2995	19.8112	21.9875	20.3140	21.4140	**22.8970**
	12	24.8107	16.7855	21.7414	25.8231	23.2965	25.9708	**26.5311**
	16	26.1256	17.0928	22.5313	27.6689	26.0409	26.8405	**28.6002**
4	4	18.5508	18.6138	17.1138	19.1078	21.4262	21.4262	**19.1378**
	8	22.9040	19.2987	18.4075	23.2655	22.0260	**23.9954**	23.5312
	12	24.3634	20.2259	20.3673	**26.5647**	24.3936	25.0019	25.1143
	16	28.0821	22.1911	23.9530	27.6167	27.8094	28.1749	**29.6135**
5	4	18.1523	16.1748	15.9589	18.7960	16.1695	18.7308	**19.4151**
	8	**23.6714**	17.6890	17.0105	23.4358	19.3198	21.1293	23.2857
	12	24.4254	19.4415	19.2915	26.6461	22.2780	25.2621	**27.1847**
	16	28.1375	21.3093	23.6164	**29.2902**	28.4748	29.4993	28.6008
6	4	16.6959	15.5516	16.4072	16.6310	16.3878	**18.3878**	16.1783
	8	22.2443	23.2185	18.3555	21.7855	21.9410	22.7283	**23.3973**
	12	25.7029	24.0306	19.7916	23.5796	24.4812	25.9510	**26.0665**
	16	28.6911	26.4871	24.9146	28.6828	28.9307	29.8234	**30.7591**

TABLE 4. The SSIM of each algorithm under Masi entropy.

IMAGE	K	CSA	GOA	CS	TLBO	EO	MPA	LCBMO-2
1	4	0.4858	0.4059	0.1263	0.5161	0.4987	0.5187	**0.5222**
	8	0.7747	0.5858	0.1928	0.8188	0.7471	0.8198	**0.8325**
	12	0.8583	0.6695	0.2662	0.8914	0.8542	0.8924	**0.9137**
	16	0.8881	0.7116	0.2764	0.9420	**0.9482**	0.9431	0.9470
2	4	0.5252	0.5559	0.3085	**0.5721**	0.5406	0.5419	0.4442
	8	0.7727	0.5938	0.3373	0.8190	0.7535	0.7720	**0.8225**
	12	0.8215	0.6360	0.3671	0.8299	0.7919	0.8465	**0.8674**
	16	0.8607	0.7830	0.7345	0.9219	0.9072	0.9287	**0.9339**
3	4	0.4071	0.3746	0.2776	0.3984	0.3206	**0.4206**	0.3984
	8	0.7169	0.5605	0.3309	0.7668	0.7543	0.7611	**0.8186**
	12	0.8316	0.6242	0.4689	0.8556	0.8102	0.8345	**0.8710**
	16	0.8758	0.7232	0.6570	0.8864	0.8909	0.8857	**0.9013**
4	4	0.5671	0.5518	0.2178	0.5844	0.5286	0.5726	**0.5850**
	8	0.7165	0.6996	0.3843	0.7088	**0.7832**	0.7190	0.7194
	12	0.7893	0.7973	0.4411	0.7337	0.8126	0.8204	**0.8356**
	16	0.8646	0.8554	0.6154	0.8481	0.8830	0.8912	**0.8995**
5	4	0.6308	0.5440	**0.6843**	0.6114	0.6296	0.6796	0.6508
	8	0.7712	0.7292	0.7596	0.7995	0.7854	0.7852	**0.8041**
	12	0.8196	0.8000	0.8332	0.8638	0.8420	**0.8681**	0.8655
	16	0.8842	0.8863	0.8807	0.8784	0.8920	0.9070	**0.9024**
6	4	0.7234	**0.7250**	0.2907	0.7219	0.7003	0.7013	0.7161
	8	0.8294	0.7604	0.3406	0.8379	0.7700	0.8114	**0.8634**
	12	**0.9000**	0.8116	0.4279	0.8975	0.8188	0.8848	0.8734
	16	0.9159	0.9364	0.5435	0.9205	0.8314	0.9270	**0.9405**

where t is the number of iteration, and λ is the initial decay rate. By solving differential Eq. (13), logistic function (14) is obtained.

$$P(t) = \frac{P_{\max}}{1 + (\frac{P_{\max}}{P_{\min}} - 1) \cdot e^{-\lambda t}} \tag{14}$$

It can be seen from (7) that $P(t) = P_{\min}$ when $t = 0$, while $P(t) = P_{\max}, t \to \infty$.

E. CHAOTIC MAP

Chaotic map is one of the best mathematical strategies to improve the performance of the metaheuristic algorithm in terms of local optima avoidance. Chaotic map can provide random behavior without the need for random component [33]. The mathematical modulation of six different chaotic maps are as following. Fig. 2 visualizes the chaotic behavior. The initial value may have a significant effect on the fluctuation patterns of some chaotic maps. Fig. 2 is drawn based on the initial value of 0.7 [71], [72].

The Chebyshev map is formulated as [73]:

$$x_{i+1} = cos(icos^{-1}(x_{i+1})) \tag{15}$$

The equation of the Gauss/mouse map is defined as follows [74]:

$$x_{i+1} = \begin{cases} 1 & x_i = 0 \\ \dfrac{1}{\mathrm{mod}(x_i, 1)} & otherwise \end{cases} \tag{16}$$

TABLE 5. The FSIM of each algorithm under Masi entropy.

IMAGE	K	CSA	GOA	CS	TLBO	EO	MPA	LCBMO-2
1	4	0.6668	0.6461	0.3363	0.6938	0.6118	**0.7406**	0.6980
	8	0.8742	0.7330	0.3878	0.9026	0.8335	0.8561	**0.9132**
	12	0.9303	0.8123	0.4514	0.9489	0.8672	0.9592	**0.9625**
	16	0.9426	0.9110	0.5667	0.9749	0.9393	0.9764	**0.9781**
2	4	0.7012	**0.7131**	0.5454	0.7051	0.7055	0.6056	0.6647
	8	0.8484	0.7917	0.6837	**0.8925**	0.8423	**0.8925**	0.8913
	12	0.8812	0.8651	0.7673	0.9179	0.8729	0.9238	**0.9280**
	16	0.9089	0.8688	0.8084	0.9605	0.9189	0.9403	**0.9692**
3	4	**0.7421**	0.7284	0.5223	0.7311	0.7099	0.7217	0.7341
	8	0.8260	0.7594	0.5255	0.8417	0.8388	0.8504	**0.8565**
	12	0.8715	0.7976	0.5928	0.8966	0.8823	0.9001	**0.9115**
	16	0.9083	0.8693	0.6978	0.9266	0.9108	0.9282	**0.9373**
4	4	0.7749	0.7640	0.5865	0.7770	**0.8276**	0.8199	**0.7776**
	8	0.8553	0.8348	0.6483	0.8543	0.8613	0.8971	**0.8609**
	12	0.8706	0.8762	0.6678	0.8652	0.8849	0.9150	**0.9026**
	16	0.9176	0.9188	0.7914	0.8965	0.9192	0.9350	**0.9353**
5	4	0.7546	0.7171	0.4890	0.7743	0.7736	0.7854	**0.7962**
	8	0.8618	0.8219	0.5408	0.8800	0.8690	0.8760	**0.8825**
	12	0.8799	0.8500	0.6386	0.9140	0.8547	0.8819	**0.9206**
	16	0.9249	0.8705	0.7515	**0.9404**	0.8787	0.9122	0.9365
6	4	0.7731	0.7714	0.7705	0.5339	0.7584	0.7418	**0.7755**
	8	0.8483	**0.8755**	0.8491	0.8500	0.8092	0.8519	0.8739
	12	0.9048	0.8918	0.8998	0.8717	0.8584	0.9052	**0.9110**
	16	0.9313	0.9262	0.9045	0.9365	0.9165	0.9477	**0.9551**

TABLE 6. The average fitness value of each algorithm at K = 16.

IMAGE	CSA	GOA	CS	TLBO	EO	MPA	LCBMO-2
1	59.0399	54.2575	56.4156	59.4657	58.9956	59.7299	**61.8733**
2	52.7597	55.9205	55.1793	53.4192	55.5071	57.9364	**59.5827**
3	55.7641	53.7352	53.9765	56.1654	56.6999	58.0864	**59.1549**
4	58.2561	57.1797	57.8783	58.6954	59.1138	60.4193	**61.2633**
5	57.0013	56.9317	56.8577	57.7764	57.9079	58.3755	**60.1861**
6	52.8967	56.5019	56.4473	53.0058	55.8742	56.6141	**57.9554**

The Logistic map is defined as [75]:

$$x_{i+1} = ax_i(1 - x_i), \quad a = 4 \tag{17}$$

The Singer chaotic map equation is expressed as [76]:

$$x_{i+1} = \mu(7.86x_i - 23.31x_i^2 + 28.75x_i^3 - 13.302875x_i^4), \quad \mu = 1.07 \tag{18}$$

The Sinusoidal map is represented by the following equation [77]:

$$x_{i+1} = ax_i^2 \sin(\pi x_i), \text{ a=2.3} \tag{19}$$

The family of Tent map can be represented as [78]:

$$x_{i+1} = \begin{cases} \dfrac{x_i}{0.7} & x_i < 0.7 \\ \dfrac{10}{3}(1 - x_i) & x_i \geq 0.7 \end{cases} \tag{20}$$

IV. PROPOSED METHOD

A. IMPROVED BARNACLES MATING OPTIMIZER (LCBMO)

Metaheuristic algorithms all have two important stages in the search level: exploration and exploitation. The balance between these two capabilities directly affects the performance of the algorithm. In the native BMO algorithm, low search accuracy and limited production capacity are the main drawbacks. In order to improve the competence of BMO algorithm to handle optimization problems, two strategies regarding logistic model and chaotic map are introduced. The pattern and mechanism of improvement will be described in details.

In the original BMO algorithm, pl can be set to 50%-70% of the total population size by repeated experiments, which is beneficial to balance the exploitation and exploration. More exploration processes will occur when the value of pl is small. On the contrary, more exploitation processes occur when the value of pl is large. Finally, the authors set pl to a constant value (70% of the population of barnacles). In view of this, the logistic model is used to improve pl to realize the adaptive transformation of parameters. The parameter is improved by the following equation.

$$pl(t) = \frac{pl_{\max}}{1 + (\frac{pl_{\max}}{pl_{\min}} - 1) \cdot e^{-\lambda t}} \tag{21}$$

It can be seen from (7) that $pl(t) = pl_{\min}$ when $t = 0$, while $pl(t) = pl_{\max}, t \rightarrow \infty$. The logistic model makes BMO algorithm to perform high exploration in the initial stage and more exploitation in the final stage of search. It can be regarded as a proper strategy to balance the two stages.

In addition, in order to avoid local optimal values, the chaotic map is used to improve the position updating equation of barnacles. Eq. (12) is replaced by the following form.

$$x_i^{n\_new} = m \times x_{barnacle\_m}^n \tag{22}$$

where m is a chaotic vector obtained based on six chaotic maps. The chaotic vector can provide random behavior without the need for random component. The purpose of introducing this strategy is to make solutions search in space as widely, randomly and globally as possible. The exploitation efficiency is the primary beneficiary. Finally, the improved version of BMO is called LCBMO whose pseudocode is provided in Algorithm 1.

The computational complexity of LCBMO depends on the related factors such as the number of barnacles N, the dimension D, the maximum number of iterations T, and the cost of fitness function F. In the initialization process, the computational complexity is $O(N)$. The computational complexity of sorting process is $O(N)$. The computational complexity can be expressed as $O(T \times N \times F)$ for fitness evaluation process and $O(T \times N \times D)$ for updating positions. The overall computational complexity of LCBMO is: $O(N \times (2{+}T \times (F + D)))$.

Algorithm 1 Pseudocode of the LCMO Algorithm

```
Initialize the population of barnacles X_i using Eq. (8)
Calculate the fitness of each barnacle
Sort to locate the best result at the top of the population
While t < Max_iter do
    Set the dynamic value of pl using Eq. (21)
    Select Dad and Mum using Eqs. (9) and (10)
    If selection of Dad and Mum = pl
        For each variable
            Generate offspring using Eq. (11)
        End for
    Else if selection of Dad and Mumpl
        For each variable
            Generate offspring using Eq. (22)
        End for
    End if
    Bring the current barnacle back if it goes outside
    boundaries
    Calculate the fitness of each barnacle
    Sort and update the best solution if there is a better
    solution
    t = t+1
End while
Return the best solution
```

B. LCBMO BASED MULTILEVEL THRESHOLDING METHOD

The process of finding the threshold by Masi entropy is actually to find the optimal solution. However, they have high computational complexity when dealing with multiple thresholds. In order to achieve efficiency, it is entirely possible to use LCBMO algorithm to deal with this. The basic steps are described as follows:

Firstly, we input selected color images and calculate the components of the histogram. Next, the number of search agents and iterations are initialized, and the fitness of initial population is calculated. The dynamic pl value is used to determine the position update mode of barnacles. Individual with high fitness value is preserved. Repeat this process until the maximum number of iterations is completed. The best position represents the optimal threshold values of segmentation. The flowchart is provided in Fig. 3.

V. BENCHMARK FUNCTIONS EXPERIMENT

In this section, 23 standard functions are used to evaluate the optimization improvement of LCBMO algorithm. These benchmark functions are divided into three groups: unimodal ($f_1 - f_7$), multimodal ($f_8 - f_{13}$) and fixed-dimension multimodal ($f_{13} - f_{23}$). Furthermore, the relevant composition, dimension, range limitation and optimal position of 23 functions can be found in [49]. Meanwhile, all the experimental series are carried out on MATLAB R2016b, and the computer is configured as AMD A8-7410 APU with AMD Radeon R5 Graphics @2.20 GHz, using Microsoft Windows 7 system. For the experiment, the most traditional and improved BMO algorithm for global optimization are adopted. And the population size is set to 30 while the number of iterations is set to 500. Moreover, all experiments are conducted 30 times.

In LCBMO, the logistic model can make the algorithm be highly explored in the initial stage and developed more in the later search period. Compared with the traditional BMO, it has excellent exploration and exploitation. For the chaotic map, putting it into BMO as a strategy can greatly improve the convergence and high efficiency. The LCBMOs are divided into 6 different types. LCBMO-1 to LCBMO-6 all introduce the logistic model, but utilize Chebyshev, Gauss/mouse, Logistic, Singer, Sinusoidal, and Tent maps, respectively. The performance of algorithms is evaluated according to the mean value and standard deviation (Std). The stability of each model is evaluated by Std value. Meanwhile, the best results has been highlighted in boldface in Table 1. It can be found from the Table 1 that the LCBMO-1, LCBMO-2, LCBMO-3, LCBMO-4, LCBMO-5 and LCBMO-6 models show much better results compared to BMO on unimodal benchmark functions. In other words, Chebyshev, Gauss/mouse, Logistic, Singer, Sinusoidal and Tent chaotic maps have successfully improved the performance of the BMO algorithm. For multimodal benchmark functions, it can be seen that the LCBMO-2 model shows the best value and great stability in most cases. Although BMO, LCBMO-1 and LCBMO-6 models show competitive result in some cases, this result still proves that the optimal solution obtained by the proposed method is high-quality. In addition, as for fixed-dimension multimodal benchmark functions, compared to other hybrid model, LCBMO-2 model can keep the population diversity in the later iteration. Therefore, the ability to avoid local optimization has enhanced. Moreover, it can be found from the Table 1 that LCBMO-2 shows the lowest value of Std, which indicates better stability. Thus, it can be said that the

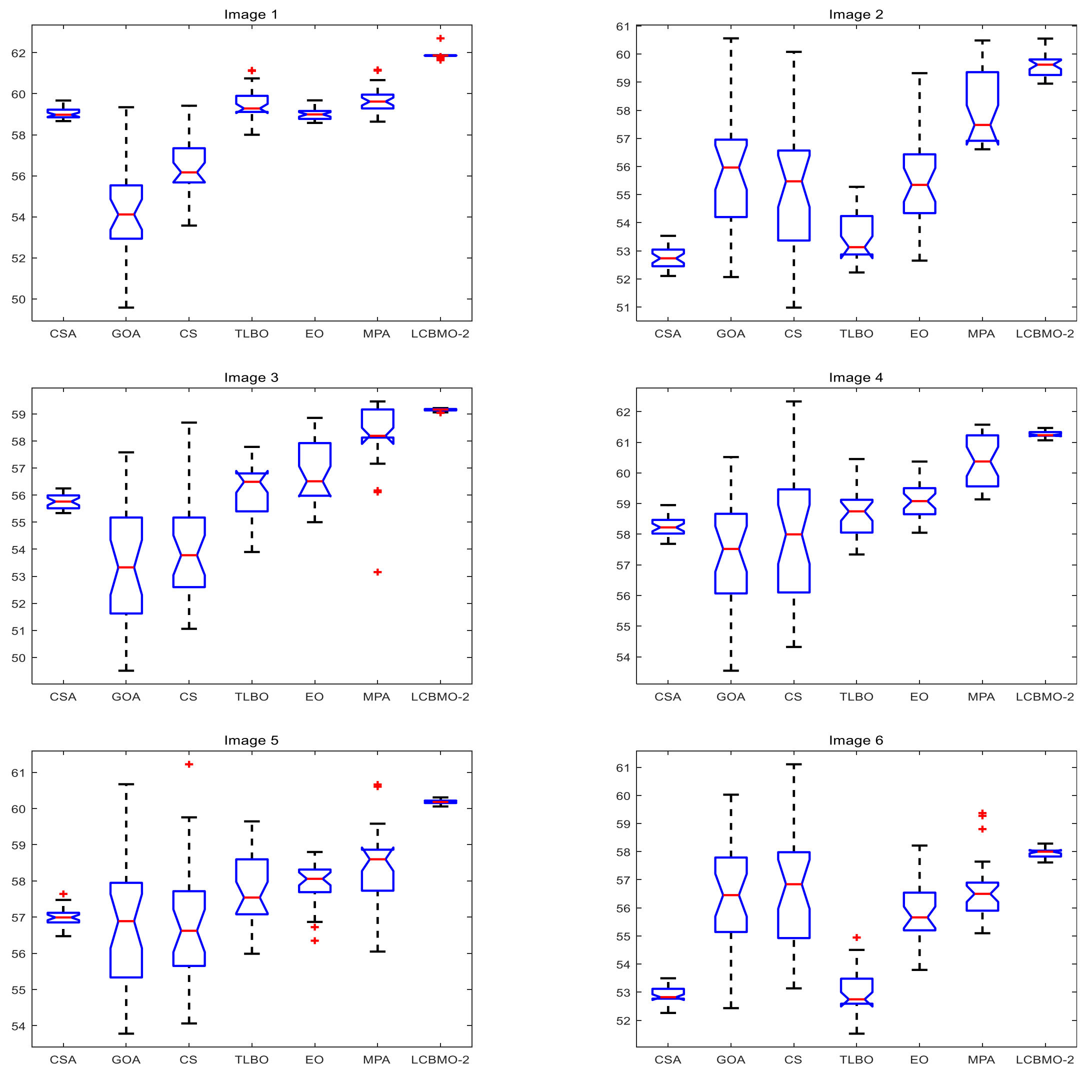

FIGURE 6. **The boxplot based on each algorithm at K = 16.**

proposed method in this article is more effective than BMO in 23 benchmark functions, so this article combines LCBMO with multilevel thresholding segmentation method to improve the image segmentation accuracy.

VI. COLOR IMAGES SEGMENTATION EXPERIMENT

A. PREPARED WORKS

1) EXPERIMENTAL SETUP

All the experimental series were carried out on MATLAB R2016b, and the computer was configured as AMD A8-7410 APU with AMD Radeon R5 Graphics @2.20 GHz, using Microsoft Windows 7 system.

2) COMPARED ALGORITHMS

After the thresholding segmentation method is extended from two-level thresholding to multi-level thresholding, its computational complexity increases exponentially. Therefore, a large number of optimization algorithms are applied in multithreshold segmentation. In order to prove the superiority of the modified algorithm, two sets of 10 meta-heuristic algorithms which have been proposed and widely applied to multithreshold segmentation are selected for comparison experiments, including MABC [48], CSA [51], GOA [52], CS [53], EO [79], MPA [80], IDSA [54], TLBO [55], WOA-TH [57], and BDE [58]. These comparison algorithms have different search strategies and mathematical formulas and are representative algorithms for multithreshold. The maximum of iterations for all algorithms is 500 and the population size is 30. We follow the same parameters in the original articles. The main parameters of various algorithms are shown in Table 2.

3) COLOR IMAGE DATABASE

In this article, two sets of twelve color images are selected from the Berkeley university database and NASA landsat image dataset for performance analysis. The satellite images

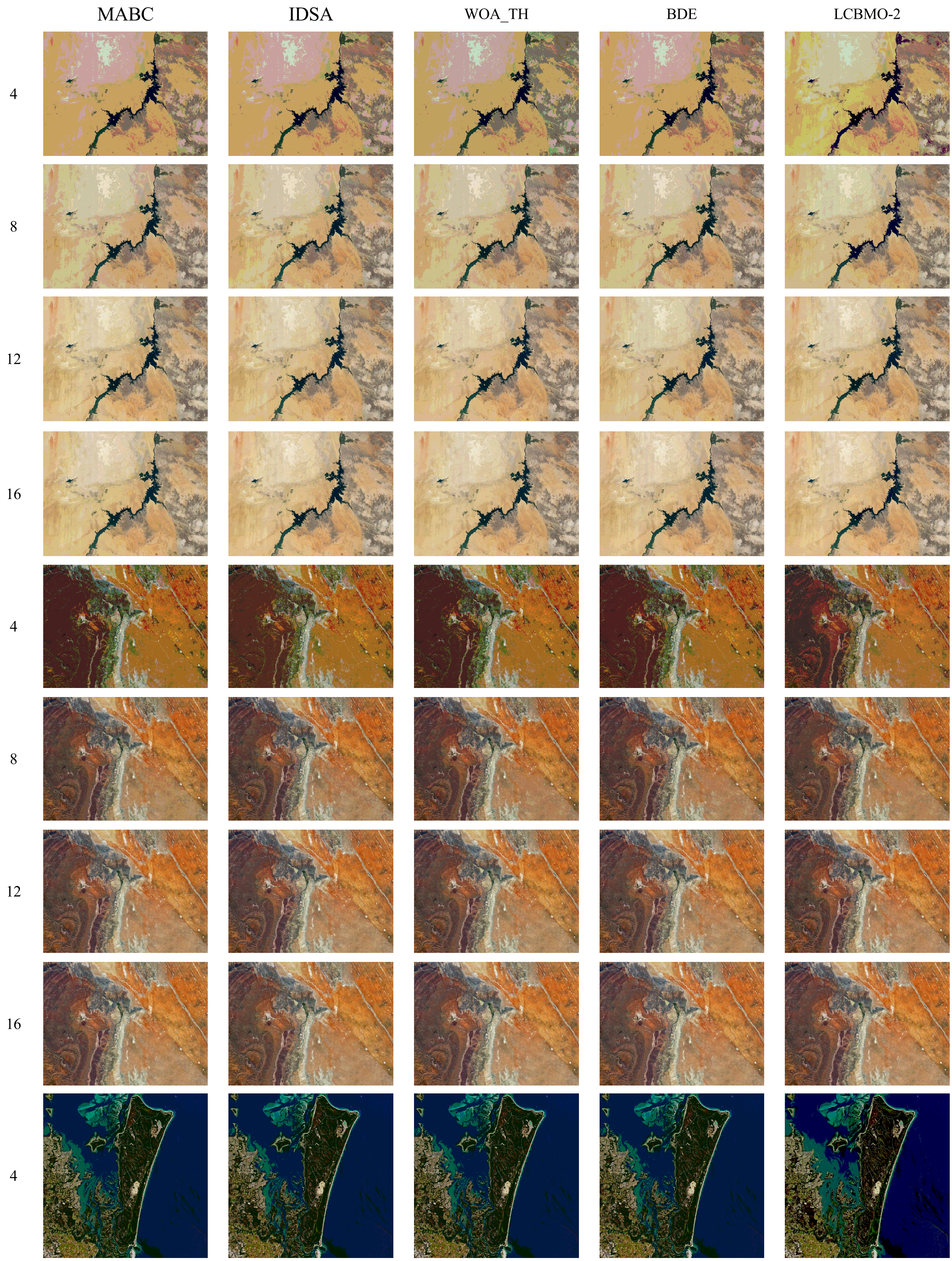

FIGURE 7. The segmentation results based on each algorithm.

FIGURE 7. ***(Continued.)*** **The segmentation results based on each algorithm.**

can be downloaded from the website [81]. Fig. 4 shows the original test images and the corresponding histograms for each of color channels (red, green, and blue). All images are in JPG format.

The experiments use the control variable method, in which each algorithm runs each image 30 times separately. The number of threshold K includes: 4, 8, 12, and 16.

B. EVALUATION METRICS

1) PEAK SIGNAL TO NOISE RATIO

The peak signal to noise ratio (PSNR) is an objective image quality evaluation algorithm based on pixel error. A higher PSNR value indicates that the quality of the distorted test image is better and closer to the original reference image. However, it is based on the error between corresponding pixels and does not take into account the visual characteristics of human eyes. Its calculation formula is as follows:

$$PSNR = 10\log_{10}\frac{L^2}{MSE}(db) \tag{23}$$

where L represents the grayscale range of the image. For 8-bit grayscale image, $L = 255$. MSE is the mean square error between the original image and the processed image.

$$MSE = \frac{\sum_{m=1}^{M}\sum_{n=1}^{N}[R(m,n) - I(m,n)]^2}{M \times N} \tag{24}$$

where $M \times N$ is the size of the image, $R(m, n)$ represents the gray value of coordinates at the reference image (m, n), and $I(m, n)$ represents the gray value of coordinates at the distorted image (m, n).

2) STRUCTURAL SIMILARITY INDEX

It is an objective image quality evaluation algorithm based on structural similarity. It measures the image similarity from brightness, contrast and structure. SSIM value range is [0, 1]. If the value is closer to 1, the image distortion is smaller. It is defined as follows

$$SSIM(R,I) = \frac{(2\mu_R\mu_I + C_1)(2\sigma_{RI} + C_2)}{(\mu_R^2 + \mu_I^2 + C_1)(\sigma_R^2 + \sigma_I^2 + C_2)} \tag{25}$$

where U_R and U_I are the average gray values of the original image R and the segmented image I. σ_R^2 and σ_I^2 represent the variance of image R and image I respectively. σ_{RI} is the covariance of image R and image I. $C_1 = (0.01L)^2$, $C_2 = (0.03L)^2$.They are constants that are used to maintain stability.

3) FEATURE SIMILARITY INDEX

On the basis of SSIM, researchers have proposed a new image quality assessment metric based on underlying features, namely feature similarity algorithm (FSIM). Researchers use two complementary features of phase congruency (PC) and gradient magnitude (GM) to calculate FSIM.

$$FSIM = \frac{\sum_{x\in\Omega} S_L(x) \times PC_m(x)}{\sum_{x\in\Omega} PC_m(x)} \tag{26}$$

where Ω is the pixel field of the entire image, $S_L(x)$ represents the similarity value of each position x,and $PC_m(x)$ denotes the phase consistency measure.

$$S_L(x) = [S_{PC}(x)]^{\alpha} \cdot [S_G(x)]^{\beta} \tag{27}$$

$$PC_m(x) = \max(PC_1(x), PC_2(x)) \tag{28}$$

TABLE 7. Comparison of optimal thresholds of each algorithm.

IMAGE	K	MABC			IDSA		
		R	G	B	R	G	B
7	4	43 114 158 200	56 105 161 222	36 94 158 193	41 114 158 200	57 106 161 222	36 94 158 193
	8	21 50 80 111 137 173 203 239	27 51 77 106 137 165 196 22	20 40 66 90 115 140 165 197	21 53 86 111 137 176 208 239	26 51 77 106 139 167 195 223	20 42 64 90 116 149 170 196
	12	16 31 52 76 93 112 131 149 179 203 221 238	25 51 73 96 122 139 156 173 191 204 218 230	15 36 60 79 96 112 134 149 174 191 212 225	15 37 55 71 91 111 131 152 174 198 217 238	28 50 74 97 114 133 152 166 187 205 222 238	24 39 51 69 89 107 129 152 174 192 208 225
	16	14 25 37 60 72 89 108 119 129 147 163 177 203 217 235 247	22 35 46 55 77 92 109 123 140 148 158 179 191 205 225 239	11 26 40 50 63 77 91 111 132 157 171 181 191 211 220 227	22 34 57 69 82 99 115 130 148 166 184 198 211 224 234 243	26 48 63 76 90 104 113 127 141 159 174 190 205 212 229 240	14 23 30 42 63 76 91 105 121 138 155 172 187 199 213 225
8	4	41 70 163 222	32 106 168 218	31 122 165 210	52 83 163 222	41 107 165 217	31 122 165 210
	8	26 56 79 111 145 176 207 232	29 52 78 111 140 171 205 233	25 50 80 113 142 171 201 226	23 43 70 99 133 170 202 230	29 51 80 112 145 174 205 233	25 49 79 107 133 160 185 210
	12	17 38 56 76 100 122 141 157 175 193 215 234	27 42 61 81 101 123 145 166 181 205 216 236	16 30 54 76 95 116 135 154 176 194 209 228	21 42 56 73 92 121 144 159 174 195 220 235	29 43 62 87 107 133 152 171 190 209 228 240	21 41 58 77 97 116 136 151 165 185 205 226
	16	17 29 41 48 64 81 101 113 129 149 161 171 191 211 226 237	19 30 43 57 79 92 104 116 133 150 167 182 195 209 228 250	17 36 52 68 75 99 108 125 139 154 168 183 197 210 220 232	15 28 43 58 77 91 102 112 125 142 153 169 180 206 224 235	27 41 54 66 79 90 100 113 130 151 171 188 205 218 228 243	15 32 51 72 93 111 134 144 157 167 179 191 203 219 229 241
9	4	68 119 164 202	64 115 158 194	33 86 138 183	71 122 169 202	68 121 164 197	33 86 138 183
	8	4 38 77 107 139 171 197 225	30 57 89 116 145 169 194 224	31 58 82 107 133 157 183 211	5 44 82 107 137 170 199 226	30 61 88 114 142 168 194 227	32 60 86 112 139 167 197 230
	12	4 30 52 77 92 113 137 164 182 199 215 234	28 49 72 94 113 135 149 167 183 195 214 233	21 36 53 76 94 122 138 157 175 190 208 230	5 31 54 74 92 109 128 150 165 187 210 236	26 42 60 77 96 119 137 156 174 194 213 228	26 48 65 81 96 111 128 142 162 179 200 225
	16	6 18 33 47 62 72 91 122 136 148 161 178 193 208 222 241	9 22 36 54 68 92 105 115 138 154 169 177 193 210 223 243	16 25 37 50 66 78 91 105 114 124 141 167 185 198 223 241	4 18 32 46 58 73 88 108 125 140 157 175 192 212 225 241	21 33 48 62 74 86 98 108 125 146 162 179 195 213 228 245	7 30 51 69 83 96 112 126 133 148 164 177 191 200 216 233
10	4	59 108 158 202	26 92 141 193	68 112 154 197	58 104 158 204	26 97 152 197	68 112 155 197
	8	28 55 83 112 139 169 199 225	23 45 78 110 139 167 193 221	22 48 75 108 132 162 190 215	29 54 77 102 141 180 205 229	23 46 77 105 131 161 191 220	24 50 77 107 130 154 178 206
	12	29 47 63 82 99 118 136 152 170 193 211 231	12 25 44 58 81 102 122 142 160 184 203 228	18 32 52 71 94 105 120 140 161 187 203 222	22 47 64 84 104 118 138 158 176 194 209 231	19 38 52 72 92 111 128 151 166 185 203 225	19 33 48 65 81 100 115 134 156 179 201 224
	16	14 31 45 56 77 100 115 135 155 178 187 197 205 214 227 241	12 29 42 54 67 80 98 107 123 143 159 170 201 215 225 240	14 26 40 50 59 82 94 107 125 141 156 167 178 192 211 227	18 34 50 65 81 95 111 124 137 150 164 178 191 202 217 235	12 26 41 54 69 79 91 107 123 140 157 173 190 204 220 233	22 39 56 73 90 105 120 135 152 170 189 201 212 223 233 242
11	4	58 102 146 223	60 112 173 220	50 84 142 211	58 102 146 223	61 112 173 221	48 84 138 209
	8	33 62 88 112 138 164 197 228	32 60 88 116 143 175 200 227	37 64 86 113 139 167 196 223	30 63 95 122 148 173 200 231	39 69 97 125 151 179 207 231	32 51 79 107 138 167 198 224
	12	20 45 64 91 109 124 141 160 179 200 222 242	19 38 55 75 94 110 132 155 172 193 216 235	25 43 60 81 102 121 141 158 185 205 222 236	24 44 66 85 104 123 141 158 177 196 216 237	23 41 61 83 102 122 141 160 179 196 216 237	34 51 70 88 107 121 136 154 174 191 209 229
	16	16 33 49 66 71 80 101 114 125 146 161 180 193 212 226 238	27 40 52 70 79 92 106 119 132 154 170 178 200 211 228 244	22 31 49 65 78 106 123 133 142 158 167 181 192 204 222 241	16 32 49 61 78 95 114 131 146 164 179 198 211 220 232 245	23 40 58 72 85 93 105 121 138 154 176 190 205 218 229 242	13 27 41 58 75 89 105 120 135 147 161 175 191 205 222 239
12	4	57 103 156 205	42 82 143 197	29 65 121 195	53 100 152 201	42 82 143 197	29 65 121 195
	8	14 45 76 103 132 165 197 228	25 48 79 109 140 170 198 229	26 46 72 104 132 163 192 219	13 43 75 105 133 164 196 228	34 56 82 112 142 171 201 230	21 47 74 109 143 174 205 230
	12	18 34 50 67 84 102 126 147 174 195 217 236	21 38 54 71 86 109 131 147 166 187 212 231	17 36 55 72 89 112 128 150 173 193 215 232	11 33 51 70 86 107 129 152 173 196 220 236	23 42 58 76 92 110 127 149 168 190 210 233	17 34 49 66 79 91 104 125 151 178 205 230
	16	11 23 36 58 68 86 104 129 143 161 172 184 198 208 221 234	19 30 46 64 85 101 118 124 146 165 173 186 196 210 225 235	16 29 48 60 81 101 119 128 140 154 163 173 188 204 226 238	9 25 40 58 73 84 96 112 126 140 153 173 193 213 228 242	12 22 35 46 62 77 92 103 116 133 149 166 183 195 211 231	14 30 45 55 66 87 102 117 134 147 161 175 189 201 216 233

where $S_{PC}(x)$ is the similarity measure of phase consistency, $S_G(x)$ represents the similarity measure of gradient magnitude, and α, β are both constants.

$$S_{PC}(x) = \frac{2PC_1(x) \times PC_2(x) + T_1}{PC_1^2(x) \times PC_2^2(x) + T_1} \tag{29}$$

$$S_G(x) = \frac{2G_1(x) \times G_2(x) + T_2}{G_1^2(x) \times G_2^2(x) + T_2} \tag{30}$$

where T_1 and T_2 are positive constants that increase stability.

4) WILCOXON RANK-SUM TEST

Wilcoxon rank-sum test is used to compare the two samples. The p value returned represents the probability whether two independent samples are identical, and the h value returned represents the result of hypothesis test. The null hypothesis H_0 represents the statement of no difference. At significance level 5%, it generally believe that if p <0.05(or $h = 1$) means rejection of the null hypothesis, if p >0.05 (or $h = 0$) means that H_0 cannot be rejected at the 5% level.

TABLE 8. The PSNR of each algorithm under Masi entropy.

IMAGE	K	MABC	IDSA	WOA_TH	BDE	LCBMO-2
7	4	18.2007	18.2114	17.2563	18.2007	**19.1160**
	8	23.6300	23.6540	23.7105	23.8559	**24.2969**
	12	**27.6018**	27.0490	27.4933	26.8865	27.1574
	16	27.9356	29.7352	29.6724	30.1504	**30.1521**
8	4	15.3576	16.1202	15.3576	15.5939	**16.8826**
	8	23.3730	23.3871	22.7854	23.0168	**23.4774**
	12	26.8710	26.7478	26.9868	**27.1873**	25.7287
	16	28.6141	28.1745	28.6406	29.2417	**29.7247**
9	4	19.1021	18.7466	19.0644	16.5387	**19.1081**
	8	24.0016	23.9694	**24.2659**	23.6486	20.0786
	12	26.8760	27.0653	24.6080	27.4009	**27.5735**
	16	29.5999	29.1155	29.4242	28.3301	**30.1050**
10	4	16.5265	17.5688	17.5348	17.5374	**17.7046**
	8	24.0391	**24.3097**	24.1835	24.2300	22.4801
	12	26.9152	27.4526	25.4049	27.3150	**27.6707**
	16	29.3430	29.3776	29.6925	27.9892	**30.2118**
11	4	18.0895	18.0619	18.0895	18.1319	**18.2625**
	8	23.3103	23.8757	23.5759	23.7345	**24.9803**
	12	27.1949	26.8338	27.0993	26.2429	**28.1751**
	16	28.2634	29.5835	29.5607	29.1181	**30.3144**
12	4	18.3298	18.3645	18.3298	**18.4089**	18.3298
	8	23.5761	23.6314	23.4507	23.5774	**23.7936**
	12	26.8188	26.8561	27.1105	26.0924	**27.1363**
	16	28.5066	28.9744	29.5627	29.2562	**29.7149**

TABLE 9. The SSIM of each algorithm under Masi entropy.

IMAGE	K	MABC	IDSA	WOA_TH	BDE	LCBMO-2
7	4	0.6809	0.6815	0.6566	0.6809	**0.6847**
	8	0.7948	0.7856	0.7969	0.7988	**0.8090**
	12	**0.8658**	0.8538	0.8648	0.8571	0.8605
	16	0.8704	0.9016	0.9025	0.9064	**0.9091**
8	4	0.4962	0.5312	0.4962	0.5071	**0.5769**
	8	0.8289	0.8340	0.8139	0.8218	**0.8366**
	12	0.9110	0.9071	0.9140	0.8869	**0.9176**
	16	0.9320	0.9270	0.9349	0.9456	**0.9508**
9	4	0.6243	0.6068	0.6218	**0.6244**	0.4067
	8	0.8112	0.8090	**0.8194**	0.8028	0.6177
	12	0.8647	0.8640	0.8699	0.8742	**0.8766**
	16	0.9246	0.9002	0.8954	0.9439	**0.9444**
10	4	**0.5153**	0.5105	0.5085	0.5086	0.4158
	8	0.7745	0.7789	0.7799	0.7083	**0.7802**
	12	0.8328	0.8495	**0.8669**	0.8563	0.8022
	16	0.8993	0.8921	0.9016	0.8657	**0.9103**
11	4	0.7098	0.7093	0.7098	0.7113	**0.7192**
	8	0.8532	0.8684	0.8609	0.8652	**0.8959**
	12	0.9250	0.9176	0.9230	0.9032	**0.9408**
	16	0.9306	0.9509	0.9500	0.9446	**0.9596**
12	4	0.7665	0.7681	0.7665	0.7665	**0.7700**
	8	0.9035	0.9048	0.9017	0.9038	**0.9080**
	12	0.9447	0.9466	**0.9491**	0.9358	0.9485
	16	0.9584	0.9631	0.9672	0.9650	**0.9690**

5) FRIEDMAN TEST

Non-parametric Friedman test is applied to estimate which algorithms have significant differences. This multiple comparison can be used for comparisons between more than two algorithms and ranks the each algorithm separately.

C. BERKELEY IMAGES SEGMENTATION EXPERIMENT

This subsection analyzes the results provided by Masi entropy implementations based on CSA, GOA, CS, TLBO, EO, MPA, and LCBMO-2, after being applied to segment the 6 Berkeley images (image 1-6). Fig. 5 represents segmented images into four classes using LCBMO-2 algorithm and the fitted histogram with the thresholds for the segmented images. The Berkeley images are segmented using Eq. (6) and the best threshold values found by the LCBMO-2. Fig. 5 visually shows the search capabilities of LCBMO-2 in K-dimensional search space.

Table 3-5 report PSNR, SSIM, and FSIM from the evaluation of the segmented images, respectively. From the Table 3, we can observe that the LCBMO-2 based method gives the higher PSNR values in general, which indicates that the segmented image is similar to the original image. For example, in the image 6 through Masi technique (for K = 16), the PSNR values are 28.6911, 26.4871,

TABLE 10. The FSIM of each algorithm under Masi entropy.

IMAGE	K	MABC	IDSA	WOA_TH	BDE	LCBMO-2
7	4	0.7321	0.7326	0.7029	0.7321	**0.7446**
	8	0.8481	0.8434	0.8509	0.8539	**0.8651**
	12	0.9139	0.9073	**0.9146**	0.9089	0.9111
	16	0.9184	0.9427	0.9400	0.9497	**0.9507**
8	4	0.6557	0.6827	0.6557	0.6653	**0.7204**
	8	0.9150	0.9141	0.9047	0.9093	**0.9153**
	12	0.9588	0.9563	0.9613	0.9471	**0.9621**
	16	0.9678	0.9669	0.9717	0.9743	**0.9781**
9	4	**0.9102**	0.8914	0.8985	0.9002	0.8238
	8	0.9651	0.9637	0.9186	0.9629	**0.9674**
	12	0.9775	0.9757	0.9682	0.9798	**0.9803**
	16	0.9877	0.9836	0.9847	**0.9885**	0.9830
10	4	0.8823	**0.8786**	0.8780	0.8780	0.8582
	8	0.9603	0.9617	0.9621	0.9407	**0.9628**
	12	0.9739	0.9812	**0.9823**	0.9813	0.9707
	16	0.9850	0.9877	0.9894	0.9832	**0.9903**
11	4	0.8931	0.8936	0.8931	0.8940	**0.8959**
	8	0.9606	0.9672	0.9644	0.9666	**0.9754**
	12	0.9857	0.9832	0.9850	0.9746	**0.9892**
	16	0.9890	0.9921	0.9917	0.9903	**0.9933**
12	4	0.9223	0.9223	0.9223	**0.9230**	0.9223
	8	0.9769	0.9782	0.9765	0.9775	**0.9794**
	12	0.9882	0.9878	0.9887	0.9860	**0.9897**
	16	0.9914	0.9923	0.9935	0.9935	**0.9942**

TABLE 11. The average fitness value of each algorithm.

IMAGE	K	MABC	IDSA	WOA_TH	BDE	LCBMO-2
7	4	**30.4982**	30.4976	30.0127	**30.4982**	30.4882
	8	42.6620	42.5971	42.3578	42.6572	**42.6741**
	12	51.8025	52.1063	50.9048	52.2167	**52.2504**
	16	58.8019	59.2167	57.3708	59.9432	**60.0104**
8	4	**30.7294**	30.7023	30.6794	30.7287	**30.7294**
	8	43.7170	43.5701	43.5403	43.7440	**43.7504**
	12	53.2312	53.2168	52.5576	53.3588	**53.5073**
	16	60.4396	60.4510	59.7813	60.9434	**61.3517**
9	4	**31.3420**	31.3324	31.0421	**31.3420**	31.3410
	8	43.7958	43.7180	42.9805	43.7823	**43.8202**
	12	53.1768	53.1099	51.7778	53.3948	**53.4618**
	16	60.2456	60.4285	60.3254	61.0127	**61.1725**
10	4	31.8139	31.8132	31.6638	**31.8146**	31.8132
	8	44.1346	44.0643	43.9029	44.1377	**44.1476**
	12	53.2432	53.3130	53.1202	53.2639	**53.4773**
	16	60.2350	60.9759	59.7542	61.1469	**61.3551**
11	4	**32.6256**	32.6183	32.5119	32.6180	**32.6256**
	8	44.9539	44.8619	44.2172	44.9669	**44.9759**
	12	54.1653	54.2734	53.8891	54.0886	**54.3966**
	16	61.0911	61.7204	61.4387	62.0976	**62.1485**
12	4	**31.8183**	31.8182	**31.8183**	31.8138	**31.8183**
	8	44.1536	44.0927	44.0938	**44.1695**	44.1584
	12	53.5618	53.5294	53.2184	53.1146	**53.8210**
	16	60.6674	61.2279	61.1520	61.4314	**61.6188**

24.9146, 28.6828, 28.9307, and 29.8234 for CSA, GOA, CS, TLBO, EO, and MPA respectively. Besides, it can be seen from the Table 4 that LCBMO-2 based method outperform the other algorithms again, which shows the segmentation accuracy of proposed algorithm is satisfied. On comparing the FSIM values, which are given in Table 5, it can be observed that the values increase as the number of the thresholds increase. And the proposed method gives the highest values, accounting for 75% of the total results. These results indicate the precise search ability of LCBMO-2 based method, which is suitable for color Berkeley images segmentation.

As the stochastic nature of metaheuristic algorithms, the experiments are conducted over 30 runs. Then the average fitness values at K = 16 are presented in Table 6. It can be seen from the tables above that the LCBMO-2 based method gives all the best values. In order to verify the stability of proposed algorithm, the results of the fitness function values at K = 16 obtained for 30 runs is plotted as boxplots. A narrower boxplot indicates better stability. The boxplots obtained by all algorithms are shown in Fig. 6. From the figure it is found that LCBMO-2 based method gives narrower boxplots as compared to other algorithms, which shows the better consistency and stability of proposed algorithm.

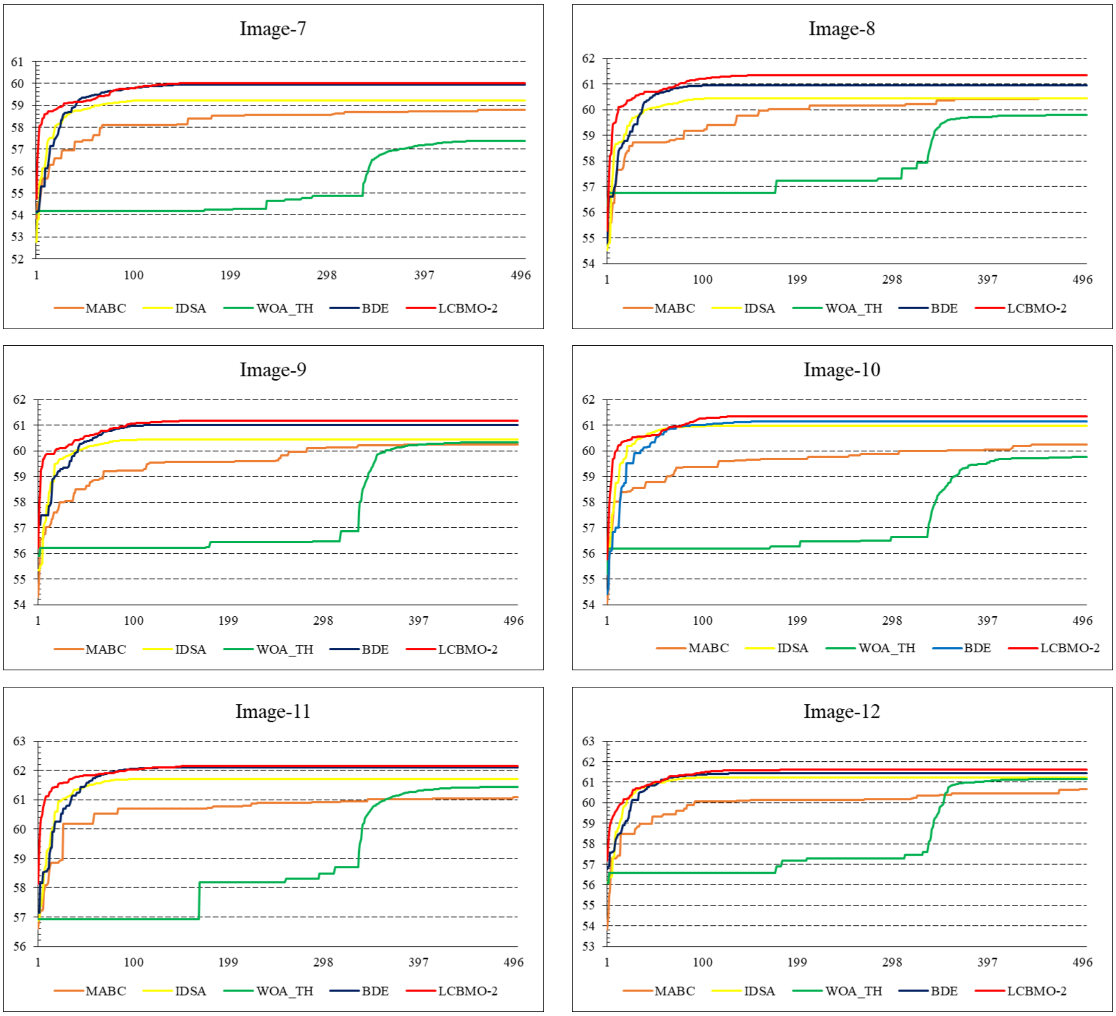

FIGURE 8. The convergence curve of fitness values for each algorithm at K = 16.

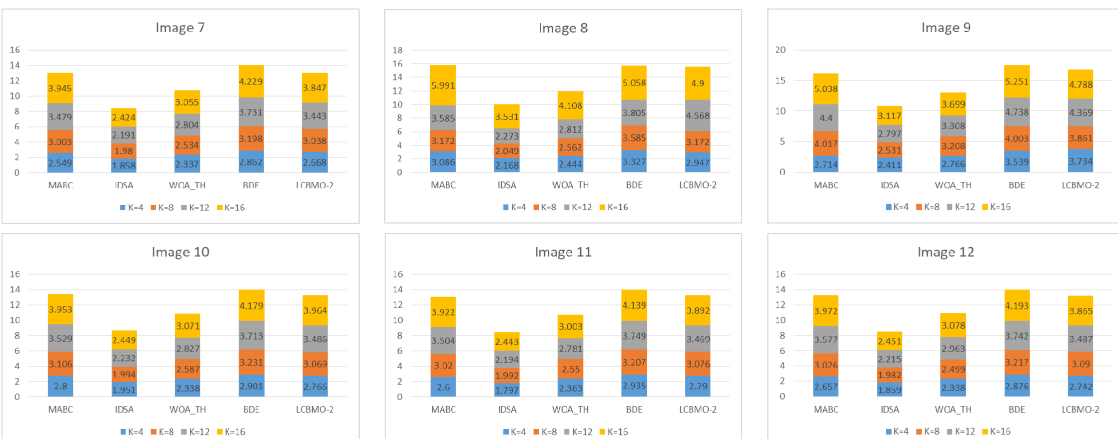

FIGURE 9. The running time (in second) based on each algorithm.

D. SATELLITE IMAGES SEGMENTATION EXPERIMENT

With the progress of earth observation technology and the deepening of understanding of earth resources and environment, the requirements for the quality and quantity of high-resolution remote sensing data are constantly increasing. The main features of high-resolution satellite images

TABLE 12. The *p* values of Wilcoxon rank-sum test.

IMAGE	K	MABC	IDSA	WOA_TH	BDE
7	4	3.16E-21	7.65E-101	8.26E-46	7.97E-67
	8	2.02E-53	3.03E-122	1.55E-90	2.81E-91
	12	7.19E-94	1.94E-125	3.45E-158	3.28E-103
	16	5.42E-148	5.42E-148	1.05E-166	6.85E-162
8	4	5.61E-10	3.41E-51	**0.1277**	6.43E-83
	8	1.14E-54	4.86E-67	1.52E-12	4.17E-106
	12	2.19E-91	9.32E-92	7.08E-75	9.42E-139
	16	8.34E-104	8.34E-104	9.18E-162	5.86E-155
9	4	7.54E-05	2.51E-11	2.32E-102	6.19E-47
	8	1.68E-14	8.49E-22	7.08E-55	2.75E-104
	12	2.13E-26	3.92E-35	6.21E-114	1.93E-131
	16	2.60E-37	2.60E-37	4.62E-159	5.56E-155
10	4	2.95E-91	1.72E-65	**0.0550**	8.80E-62
	8	1.63E-16	5.22E-84	4.76E-03	1.56E-127
	12	8.41E-83	7.69E-102	1.44E-171	8.92E-109
	16	5.80E-106	5.80E-106	5.80E-164	1.40E-154
11	4	6.88E-08	8.51E-32	2.57E-05	6.31E-19
	8	1.27E-08	5.98E-15	8.18E-86	3.68E-71
	12	8.26E-13	1.09E-24	1.93E-153	8.72E-88
	16	7.25E-28	7.25E-28	4.90E-165	3.48E-152
12	4	**0.0928**	2.81E-57	1.79E-111	8.24E-49
	8	7.94E-05	4.52E-15	7.35E-86	6.93E-93
	12	1.57E-18	1.46E-43	9.01E-133	1.73E-127
	16	8.12E-26	8.12E-26	1.25E-144	6.38E-149

TABLE 13. The results of ranks of Friedman test.

IMAGE	MABC	IDSA	WOA_TH	BDE	LCBMO-2
7	3.4000	3.0500	3.4000	3.2000	**1.9500**
8	3.4750	2.9500	3.5750	3.2500	**1.7500**
9	2.7750	3.2000	3.4000	3.0250	**2.6000**
10	3.5000	2.5750	2.9750	3.5750	**2.3750**
11	3.7000	2.6500	3.4250	3.7000	**1.5250**
12	3.7750	2.7250	3.0000	3.5750	**1.9250**

include: rich texture information corresponding to objects, large imaging spectrum, and short revisit time. Therefore, the segmentation and evaluation of satellite images is a challenging work.

This subsection analyzes the results provided by Masi entropy implementations based on MABC, IDSA, WOA_TH, BDE and LCBMO-2, after being applied to segment the 6 satellite images (image 7-12). The segmented images (image 7, image 8, and image 10) obtained by Masi entropy with different thresholds levels are given in Fig. 7. Besides, the corresponding threshold values are given in Table 7 and Appendix Table 2. From the segmentation results we can find that the images with higher levels (such as K = 8, 12, and 16) contain more information than the others.

The PSNR, SSIM, and FSIM values obtained by all algorithms using Masi entropy techniques are reported in Tables 8-10. In terms of PSNR values, the proposed algorithm gives the highest values, accounting for 79.2% of the total results. Besides, the proposed algorithm gives the highest SSIM and FSIM values, accounting for 75% of the total results. Taking Image 12 (at K = 12) as an example, WOA_TH algorithm achieves the highest SSIM value of 0.9491. Our proposed algorithm ranks second and is not much different from the results obtained by WOA_TH. The average fitness values of Masi entropy functions are presented in Table 11. It can be seen from the table above that the LCBMO-2 based method gives the best values in general. Moreover, in order to reflect the performance of LCBMO-2 more intuitively, the convergence curves of Masi entropy functions (for K = 16) are shown in Fig. 8. It can be found that the proposed algorithm outperforms other algorithms in general. In other words, the LCBMO-2 based method gives higher position curves using Masi entropy technique. It is further proved that the two strategies

TABLE 14. The PSNR of LCBMO-2 algorithm under each object function.

IMAGE	K	Otsu	Mcet	Kapur	Tsallis	Masi
1	4	**21.0643**	8.1780	18.6482	17.7794	17.0351
	8	22.0930	8.1780	22.2207	20.8764	**24.0551**
	12	26.6758	8.1780	26.3194	24.8967	**27.4720**
	16	29.0852	8.1780	27.1408	28.3791	**29.9519**
3	4	**19.3636**	8.1220	15.5506	14.3611	14.4094
	8	21.6250	8.5306	20.6919	18.9631	**22.8970**
	12	25.2523	8.5883	23.5096	24.3285	**26.5311**
	16	28.1631	8.9736	24.6163	25.7160	**28.6002**
5	4	19.1016	5.2961	19.1516	18.6865	**19.4151**
	8	21.2904	5.3144	23.1143	23.1302	**23.2857**
	12	26.7551	5.3144	26.1639	26.5678	**27.1847**
	16	28.6101	5.4066	**28.7435**	28.2613	28.6008
7	4	17.7511	3.3848	18.7211	19.0463	**19.1160**
	8	21.0080	3.4649	21.8492	22.6915	**24.2969**
	12	25.5862	3.5848	24.9117	25.8671	**27.1574**
	16	29.9833	3.7008	30.2542	**30.7179**	30.1521
9	4	18.1977	11.0181	19.1055	16.5115	**19.1081**
	8	22.0751	11.0502	**22.5411**	21.9235	20.0786
	12	25.3509	11.0882	25.1386	26.3663	**27.5735**
	16	28.2492	11.2574	27.0882	28.3073	**30.1050**
11	4	**19.3968**	2.0277	18.6145	18.2153	18.2625
	8	24.1931	2.0420	24.7042	24.1126	**24.9803**
	12	26.6364	2.0420	27.8858	28.0313	**28.1751**
	16	30.2693	2.0554	30.0289	29.6196	**30.3144**

TABLE 15. The SSIM of LCBMO-2 algorithm under each object function.

IMAGE	K	Otsu	Mcet	Kapur	Tsallis	Masi
1	4	**0.6735**	0.0083	0.6089	0.5532	0.5222
	8	0.7843	0.0083	0.7690	0.7250	**0.8325**
	12	0.8206	0.0083	0.8898	0.8569	**0.9137**
	16	0.9436	0.0083	0.9046	0.9240	**0.9470**
3	4	0.3768	0.0426	**0.4548**	0.3962	0.3984
	8	0.7810	0.1071	0.7054	0.6474	**0.8186**
	12	0.8243	0.1142	0.8034	0.8237	**0.8710**
	16	0.8869	0.1996	0.8173	0.8373	**0.9013**
5	4	0.6142	0.0123	0.6107	0.6397	**0.6508**
	8	0.8033	0.0156	0.7564	0.7584	**0.8041**
	12	0.8548	0.0156	0.8344	0.8450	**0.8655**
	16	0.8829	0.0310	0.8912	0.8841	**0.9024**
7	4	0.6235	0.0071	0.6817	**0.6955**	0.6847
	8	0.7463	0.0146	0.7998	0.8057	**0.8090**
	12	0.8790	0.0271	0.8455	0.8393	**0.8605**
	16	0.8910	0.0391	**0.9104**	0.9099	0.9091
9	4	**0.7964**	0.0855	0.6198	0.4256	0.4067
	8	**0.8632**	0.0952	0.7599	0.7367	0.6177
	12	**0.9153**	0.0960	0.8082	0.8551	0.8766
	16	0.9289	0.1005	0.8632	0.8816	**0.9444**
11	4	0.6758	0.0019	0.7123	0.7110	**0.7192**
	8	0.8053	0.0029	0.8874	0.8732	**0.8959**
	12	0.9275	0.0029	0.9371	0.9367	**0.9408**
	16	0.9342	0.0038	0.9418	0.9550	**0.9596**

TABLE 16. The FSIM of LCBMO-2 algorithm under each object function.

IMAGE	K	Otsu	Mcet	Kapur	Tsallis	Masi
1	4	**0.8293**	0.3330	0.7494	0.7149	0.6980
	8	0.9114	0.3330	0.8725	0.8425	**0.9132**
	12	0.9501	0.3330	0.9478	0.9314	**0.9625**
	16	0.9653	0.3330	0.9585	0.9645	**0.9781**
3	4	0.7277	0.4254	0.7071	0.7291	**0.7341**
	8	0.8107	0.4280	0.8272	0.8085	**0.8565**
	12	0.9030	0.4283	0.8621	0.8818	**0.9115**
	16	0.9355	0.4297	0.8890	0.9033	**0.9373**
5	4	0.7974	0.4459	0.7827	0.7670	**0.7962**
	8	0.8787	0.4469	0.8565	0.8581	**0.8825**
	12	0.9148	0.4469	0.9009	0.9153	**0.9206**
	16	0.9351	0.4612	**0.9435**	0.9414	0.9365
7	4	**0.7870**	0.4952	0.7681	0.7473	0.7446
	8	0.8299	0.4952	0.8356	0.8420	**0.8651**
	12	0.9046	0.4952	0.9225	**0.9267**	0.9111
	16	0.9168	0.4953	0.9497	0.9456	**0.9507**
9	4	0.8502	0.4249	**0.8946**	0.8473	0.8238
	8	0.8749	0.4249	0.9502	0.9432	**0.9674**
	12	0.9572	0.4249	0.9564	0.9757	**0.9803**
	16	**0.9869**	0.4249	0.9782	0.9817	0.9830
11	4	0.8742	0.3275	0.8936	0.8789	**0.8959**
	8	0.9052	0.3275	0.9431	0.9384	**0.9754**
	12	0.9510	0.3275	0.9879	0.9884	**0.9892**
	16	0.9924	0.3283	0.9930	0.9915	**0.9933**

(logistic model and chaotic map) can improve the search accuracy and production capacity of the native BMO algorithm, and the LCBMO-2 algorithm can use the search space more effectively to complete the optimization task of image segmentation. For visual analysis, the results of the running time (in second) based on each algorithm are represented as stacked bar diagrams in Fig. 9. It can be seen that the running time is sorted as follows: BDE > MABC > LCBMO-2 > WOA_TH > BDE. Although our proposed algorithm is not the champion algorithm in terms of running time, it is not too bad. The improved strategy used slightly increases the computational cost of the algorithm. In general, the running time of the proposed algorithm (LCBMO-2) is acceptable.

In order to statistically prove the superior performance of the proposed algorithm, Wilcoxon rank-sum test and Friedman test are used to evaluate the significant difference among algorithms. The p values of Wilcoxon rank-sum test are given in Table 12. For example, the proposed algorithm gives better

TABLE 17. The main variables involved in this article.

Provenance	Symbols	Paraphrase
	L	The gray value
	n_i	The number of pixels with gray value of i
	N	The total number of pixels
Color images	p	The distribution probability of gray value
	k	The total number of threshold
	t	The threshold
	C	The class
	R,G,B	The three channels of color images
	ω	The probabilities of class occurrence
Masi entropy method	E	The entropy of the image
	ψ	The objective function of Kapur
	T′	Temperature profile
	t	The current iteration times
	$Max_{iteation}$	The maximum iteration times
	$\vec{A}$, $\vec{C}$	The vector of avoidance collisions
	M	The movement parameter
EPO	$\vec{P}$	The position of best optimal solution
	$\vec{P}_{ep}$	The position of other emperor penguins
	$P_{grid}(Accuracy)$	The polygon grid accuracy
	$\vec{D}_{ep}$	The distance between the emperor penguin and best fittest search agent
	$S()$	The social forces
	Pm	The mutation probability
HDPM	ub	The upper bound of parameter
	lb	The lower bound of parameter
	η_m	The distribution index
Levy Flight	S	The random step length
	T_i^{new}	The new temperature of each object
TEO	$T_i^{env.}$	The environmental temperature
	T_i^{old}	The original temperature of each object
PSNR	MSE	The mean square error
	R	The original image
	I	The segmented image
SSIM	μ_R, μ_I	The average gray values of image
	σ_R^2, σ_I^2	The variance of image
	σ_{RI}	The covariance of image
	PC	Phase congruency
	GM	Gradient magnitude
	Ω	The entire domain of image
FSIM	$S_L(x)$	The similarity value of each position x
	$PC_m(x)$	The phase consistency measure
	$S_{PC}(x)$	The similarity measure of phase consistency
	$S_G(x)$	The similarity measure of gradient magnitude
	H_0	The null hypothesis
Statistical analysis	H_1	The alternative hypothesis
	Q	The test statistic
Time complexity	O	The complexity notation

results in 23 out of 24 cases (6 images times 4 thresholds) for MABC, 24 cases for IDSA, 22 cases for WOA_TH, 24 cases for BDE. To sum up, all the other algorithms show a significant difference with LCBMO-2 based method. Table 13 ranks all algorithms based on PSNR values, SSIM values, FSIM values, fitness values, and running time. It is obvious that our proposed algorithm in the field of color image segmentation is the champion algorithm compared to other algorithms.

E. DIFFERENT OBJECTIVE FUNCTIONS EXPERIMENT

It can be seen from the above experimental results that LCBMO-2 based method is superior to other compared algorithms using Masi entropy. In order to obtain a simple and

TABLE 18. (Table 7 continued). Comparison of optimal thresholds for different algorithms using Masi entropy.

IMAGE	K	WOA_TH			BDE			LCBMO-2		
		R	G	B	R	G	B	R	G	B
7	4	24 69 115 193	56 105 161 222	36 94 158 193	43 114 158 200	56 105 161 222	36 94 158 193	53 115 159 200	109 165 193 223	56 97 158 193
	8	20 49 79 111 137 173 204 239	27 50 76 105 135 164 193 223	32 62 89 112 138 164 192 212	23 52 82 114 142 176 205 238	27 51 76 105 135 164 193 223	32 62 89 112 138 164 192 212	21 52 82 114 142 176 206 239	60 86 109 135 161 184 206 225	29 46 67 90 113 139 165 195
	12	17 41 64 88 111 130 148 167 185 203 219 239	27 50 69 87 105 124 144 164 184 205 222 237	20 36 52 69 89 106 125 146 167 192 210 225	17 37 56 74 93 111 130 150 171 193 213 239	27 50 69 87 106 125 146 166 185 205 222 237	15 32 50 68 89 108 127 147 167 192 210 225	17 41 64 88 111 133 156 178 198 216 236 246	27 51 76 105 130 149 168 186 205 221 234 248	27 54 92 112 132 153 169 185 198 212 225 256
	16	12 26 42 57 72 87 102 115 130 145 161 176 191 206 221 239	24 35 50 66 82 97 110 124 139 153 167 181 195 209 223 237	17 32 46 61 75 89 102 115 129 143 158 171 185 197 212 225	12 26 42 62 81 98 114 128 142 157 172 186 201 215 229 241	24 35 50 65 79 94 108 121 138 154 169 184 200 214 225 238	17 32 46 61 76 89 103 116 130 144 159 173 187 198 212 225	15 38 58 80 103 121 137 156 172 186 199 210 219 229 238 247	1 40 61 78 94 108 123 139 155 171 187 203 216 226 238 248	28 49 62 76 90 105 123 141 160 178 188 198 209 219 230 256
8	4	41 70 163 222	32 106 168 218	31 122 165 210	43 77 163 222	32 106 168 218	31 122 165 210	56 118 170 222	41 107 168 218	39 122 165 210
	8	26 56 79 111 142 174 207 232	29 52 87 121 156 182 209 233	25 50 85 120 147 174 201 226	26 56 79 111 142 173 206 232	29 52 86 120 154 179 207 233	25 50 83 115 143 172 201 226	41 68 92 123 151 177 207 232	38 61 93 124 156 182 209 233	25 51 86 122 152 180 205 226
	12	16 35 54 70 88 110 131 153 174 196 217 235	27 42 59 79 100 120 140 160 179 198 216 233	18 34 52 74 94 114 133 153 174 194 210 230	23 43 58 77 97 119 139 160 179 199 217 235	27 44 62 83 104 125 145 163 182 207 231 242	19 36 54 75 94 114 133 154 173 194 210 230	35 58 82 110 126 141 157 173 189 206 221 235	29 49 77 105 133 156 177 196 212 224 233 245	25 49 77 102 125 147 167 182 197 210 224 236
	16	16 29 43 56 70 84 99 115 130 146 161 176 192 207 222 235	16 29 42 55 70 86 102 118 133 149 164 179 195 212 227 241	18 31 46 60 75 89 104 119 133 147 160 174 187 201 214 230	16 30 43 56 70 83 98 113 127 144 160 175 191 206 221 235	16 30 46 61 72 83 104 124 144 160 175 190 205 218 232 243	13 21 31 42 53 66 80 97 114 131 148 166 185 205 224 242	32 52 70 84 99 115 131 147 163 174 186 198 209 220 230 240	14 30 47 64 86 105 124 142 159 176 192 208 222 233 241 248	21 39 60 80 100 117 133 150 166 180 194 206 217 227 241 255
9	4	68 119 164 202	64 115 158 194	34 89 142 183	8 119 164 202	64 115 158 194	33 86 138 183	68 119 164 202	68 121 164 197	102 147 179 211
	8	5 36 71 104 137 170 197 225	28 56 86 114 142 168 194 224	31 57 83 108 133 157 183 216	5 39 75 109 141 171 197 225	28 56 86 114 142 168 194 224	33 68 101 125 148 174 197 224	5 43 82 119 152 178 202 226	59 99 122 145 167 188 213 233	61 90 118 146 174 197 215 233
	12	4 26 47 69 90 112 134 154 175 194 214 233	26 46 66 86 106 127 146 164 181 196 214 233	20 37 54 72 91 110 128 147 166 183 203 227	4 27 50 73 94 114 135 154 175 194 214 233	26 46 66 87 104 122 141 158 178 196 218 234	20 37 55 75 95 116 135 148 166 183 204 248	7 44 87 126 148 168 183 199 214 229 241 249	9 38 67 96 122 146 167 189 204 219 233 244	32 52 71 90 109 128 148 168 186 204 224 241
	16	4 20 36 52 69 85 101 117 133 148 164 179 194 209 225 240	26 41 55 70 85 100 114 128 142 156 169 184 197 213 227 241	14 26 37 52 68 83 99 116 133 150 166 183 199 216 234 246	4 18 33 47 60 73 86 99 114 129 148 164 181 197 214 233	8 26 45 63 81 99 116 132 147 162 176 189 200 214 228 241	20 37 50 65 79 93 107 121 135 148 162 175 189 203 224 241	4 18 32 45 59 74 89 105 122 139 157 175 192 209 225 240	8 27 49 69 89 108 128 147 167 184 199 212 223 233 242 249	30 52 71 89 104 118 133 148 162 175 188 200 212 224 235 246
10	4	59 108 161 204	26 97 154 197	68 112 154 197	59 108 158 202	26 97 152 197	68 114 156 197	59 108 161 204	81 121 169 209	73 114 156 197
	8	27 54 81 111 140 169 198 225	23 45 77 107 137 166 193 221	23 49 75 107 130 156 184 212	27 56 81 109 137 166 194 223	23 45 76 102 130 159 187 218	23 49 75 108 132 162 190 216	38 62 91 120 148 177 202 227	23 45 79 112 144 173 200 224	28 72 107 130 156 178 201 221
	12	19 36 54 72 92 113 133 153 172 191 210 231	12 26 42 57 77 99 121 144 166 187 209 229	22 42 61 78 100 115 135 156 177 197 217 238	19 36 54 72 91 111 130 150 169 189 210 231	25 50 73 93 114 137 159 176 193 210 224 238	21 39 58 76 96 112 130 148 166 184 201 221	27 54 77 103 126 147 168 185 202 215 228 241	23 45 72 93 114 134 155 173 190 207 221 237	23 48 73 96 112 131 151 169 187 203 221 24
	16	16 30 45 58 73 88 104 120 136 151 165 180 194 208 223 238	12 26 40 53 70 85 100 115 130 146 161 176 191 206 221 236	18 31 46 62 77 93 107 120 135 151 166 180 194 208 223 240	16 30 46 59 72 87 101 117 132 143 155 168 193 205 219 233	12 26 38 49 60 72 87 103 118 135 152 169 187 203 220 235	18 32 48 65 80 94 107 119 133 148 162 176 190 203 220 238	18 46 65 80 96 112 128 145 162 179 191 202 213 223 233 243	6 20 35 49 72 88 104 119 135 152 169 187 204 219 233 244	19 34 51 69 85 103 119 138 157 178 200 216 228 238 242 247
11	4	58 102 146 223	60 112 173 220	50 84 142 211	58 104 147 223	61 112 173 220	50 84 142 211	58 108 148 223	60 112 173 220	65 134 177 217
	8	32 58 85 113 140 165 196 229	32 60 88 116 143 174 203 229	37 63 86 113 141 170 199 225	32 58 85 113 140 165 196 230	32 60 88 116 143 174 203 229	38 64 88 116 143 173 204 228	57 88 117 144 170 195 217 237	65 89 113 136 163 185 211 233	65 89 117 143 167 190 213 233
	12	19 38 58 77 97 117 135 155 175 196 217 237	23 41 60 79 99 119 138 158 178 199 219 237	27 45 65 84 103 122 141 160 179 198 216 234	17 35 58 77 95 114 135 155 175 195 216 235	18 52 72 90 110 129 147 166 185 204 213 228	22 38 55 74 93 113 134 153 175 195 214 232	25 48 76 101 125 148 169 188 203 218 232 244	32 60 85 108 130 150 169 185 202 216 230 243	22 38 55 74 92 116 141 165 187 204 221 237
	16	16 30 44 58 73 88 102 117 133 148 163 179 195 211 226 241	17 32 49 64 79 94 109 123 138 153 168 183 198 212 226 240	21 35 50 65 79 93 107 122 136 151 166 181 196 211 225 239	16 29 44 58 73 87 100 114 128 143 158 174 190 205 223 239	17 32 49 63 78 92 106 119 133 147 161 176 191 206 223 239	21 35 49 63 77 91 105 120 134 149 164 179 194 209 224 239	11 26 43 60 80 104 130 155 173 186 197 207 218 228 238 247	25 45 62 80 96 113 128 143 157 171 184 197 209 221 233 244	21 35 50 65 80 94 110 125 139 153 167 181 196 210 224 239
12	4	57 103 156 205	42 82 143 197	29 65 121 195	53 100 152 201	42 82 143 197	30 67 122 195	57 103 156 205	42 82 143 197	29 65 121 195
	8	14 44 75 104 135 166 197 228	25 47 78 108 139 169 200 230	17 38 66 98 127 159 191 220	15 45 75 104 135 166 197 228	25 47 78 108 139 169 200 230	26 47 72 105 134 166 197 225	15 45 75 104 135 166 197 228	27 60 88 119 148 176 204 231	26 57 86 116 145 174 203 228
	12	12 32 51 72 92 112 133 154 174 194 214 233	22 40 58 77 96 116 136 155 175 195 214 234	17 30 47 66 87 107 127 149 170 191 211 232	17 33 42 64 74 82 112 126 142 173 209 232	20 34 47 68 89 111 134 156 178 200 222 235	17 31 48 66 86 106 126 146 168 189 210 231	16 53 83 110 127 145 160 176 192 208 223 237	30 52 75 97 119 139 159 176 192 209 224 239	21 40 61 81 103 123 143 162 180 199 216 234
	16	10 25 40 55 70 85 100 115 130 145 160 175 190 205 220 235	12 25 41 57 73 87 102 117 133 148 163 178 193 208 223 238	17 30 44 58 72 87 102 117 132 147 162 177 192 207 221 236	11 29 46 60 74 88 102 116 130 144 158 174 190 206 222 236	12 23 34 48 63 78 91 103 118 137 155 173 190 208 223 238	15 26 41 60 81 100 114 126 139 152 166 180 195 211 225 238	12 33 53 71 89 107 123 139 154 168 182 195 208 220 231 241	23 41 58 77 96 114 130 145 160 175 189 202 214 226 235 244	15 27 41 56 71 87 102 117 132 148 164 179 195 211 225 238

powerful technique for color image segmentation, different thresholding techniques (different objective functions) based on LCBMO-2 is conducted in this section. Three Berkeley images and three satellite images are selected for testing. The PSNR, SSIM, and FSIM values obtained by LCBMO-2 based method using Otsu, Minimum cross entropy, Kapur entropy, Tsallis entropy, and Masi entropy are given in Tables 14-16. It can be seen that LCBMO-2 based method using Masi entropy gives higher results than using other thresholding techniques in most cases. For example, in terms of PSNR values, Masi technique presents better results in 18 out of 24 cases (6 images times 4 thresholds). Considering other two indicators, the Masi entropy technique outperforms again, in 17 cases for SSIM and 18 cases for FSIM. To sum up, these satisfied results prove that LCBMO-2 based method using Masi entropy is superior to the method using other thresholding techniques.

VII. CONCLUSION AND FUTURE WORK

In this article, the Barnacles mating optimizer algorithm based on logistic model and chaotic map for multilevel thresholding color image segmentation is proposed. Among many thresholding segmentation methods, Masi entropy method is adopted. The proposed algorithm is used to find the optimal threshold for color images. Meanwhile, 10 algorithms are selected for comparison. Objective function value, PSNR, SSIM, FSIM, Wilcoxon rank-sum test, and Friedman test are used to evaluate the segmentation quality. Firstly, by the convergence curve and boxplot at K = 16, it can be seen that LCBMO-2 algorithm can find larger objective function value more times. Then, in terms of PSNR, SSIM, FSIM, the value obtained by the LCBMO-2 algorithm is larger than other algorithms in most cases. It concludes that the segmentation performance based on LCBMO-2 algorithm is superior. Furthermore, the results of Wilcoxon rank-sum test and Friedman test demonstrate that LCBMO-2 is significantly different from other algorithms, and the improvement is effective. To sum up, a variety of experiments fully proves that LCBMO-2 algorithm has higher search accuracy and convergence speed, stronger robustness, and the overall performance of the algorithm is enhanced.

However, like other optimization algorithms, LCBMO has certain limitations. The computational complexity needs to be reduced. Runtime is important for real-world problems. The distributed island model can organize population into small independent groups (islands) and make the algorithm run in parallel. We believe that it is a potentially effective strategy to reduce the complexity. In the future, the relevant research directions are given as follows:

(1) Extend the algorithm to multi-objective problem for obtaining superior segmentation effect.

(2) Explore to introduce LCBMO-2 algorithm in other fields, such as machine learning and data mining.

APPENDIX

See Tables 17 and 18.

REFERENCES

[1] N. M. Zaitoun and M. J. Aqel, "Survey on image segmentation techniques," *Procedia Comput. Sci.*, vol. 65, pp. 797–806, Jan. 2015.

[2] M. Sridevi and C. Mala, "A survey on monochrome image segmentation methods," *Procedia Technol.*, vol. 6, pp. 548–555, Jan. 2012.

[3] A. K. M. Khairuzzaman and S. Chaudhury, "Multilevel thresholding using grey wolf optimizer for image segmentation," *Expert Syst. Appl.*, vol. 86, pp. 64–76, Nov. 2017.

[4] F. Garcia-Lamont, J. Cervantes, A. López, and L. Rodriguez, "Segmentation of images by color features: A survey," *Neurocomputing*, vol. 292, pp. 1–27, May 2018.

[5] Y. Li and X. Feng, "A multiscale image segmentation method," *Pattern Recognit.*, vol. 52, pp. 332–345, Apr. 2016.

[6] S. Eskenazi, P. Gomez-Krämer, and J.-M. Ogier, "A comprehensive survey of mostly textual document segmentation algorithms since 2008," *Pattern Recognit.*, vol. 64, pp. 1–14, Apr. 2017.

[7] L. Lalaoui, T. Mohamadi, and A. Djaalab, "New method for image segmentation," *Procedia Social Behav. Sci.*, vol. 195, pp. 1971–1980, Jul. 2015.

[8] L. He and S. Huang, "Modified firefly algorithm based multilevel thresholding for color image segmentation," *Neurocomputing*, vol. 240, pp. 152–174, May 2017.

[9] A. Dirami, K. Hammouche, M. Diaf, and P. Siarry, "Fast multilevel thresholding for image segmentation through a multiphase level set method," *Signal Process.*, vol. 93, no. 1, pp. 139–153, Jan. 2013.

[10] E. Hamuda, M. Glavin, and E. Jones, "A survey of image processing techniques for plant extraction and segmentation in the field," *Comput. Electron. Agricult.*, vol. 125, pp. 184–199, Jul. 2016.

[11] S. Kotte, R. K. Pullakura, and S. K. Injeti, "Optimal multilevel thresholding selection for brain MRI image segmentation based on adaptive wind driven optimization," *Measurement*, vol. 130, pp. 340–361, Dec. 2018.

[12] S. Hinojosa, K. G. Dhal, M. A. Elaziz, D. Oliva, and E. Cuevas, "Entropy-based imagery segmentation for breast histology using the stochastic fractal search," *Neurocomputing*, vol. 321, pp. 201–215, Dec. 2018.

[13] T. Kurita, N. Otsu, and N. Abdelmalek, "Maximum likelihood thresholding based on population mixture models," *Pattern Recognit.*, vol. 25, no. 10, pp. 1231–1240, Oct. 1992.

[14] N. R. Pal and S. K. Pal, "Image model, Poisson distribution and object extraction," *Int. J. Pattern Recognit. Artif. Intell.*, vol. 5, no. 3, pp. 459–483, Aug. 1991.

[15] N. R. Pal, "On minimum cross-entropy thresholding," *Pattern Recognit.*, vol. 29, no. 4, pp. 575–580, Apr. 1996.

[16] Y. Bazi, L. Bruzzone, and F. Melgani, "Image thresholding based on the EM algorithm and the generalized Gaussian distribution," *Pattern Recognit.*, vol. 40, no. 2, pp. 619–634, Feb. 2007.

[17] K. Hammouche, M. Diaf, and P. Siarry, "A comparative study of various meta-heuristic techniques applied to the multilevel thresholding problem," *Eng. Appl. Artif. Intell.*, vol. 23, no. 5, pp. 676–688, Aug. 2010.

[18] N. Otsu, "A threshold selection method from gray-level histograms," *IEEE Trans. Syst., Man, Cybern.*, vol. CMC-9, no. 1, pp. 62–66, Jan. 1979.

[19] C. H. Li and C. K. Lee, "Minimum cross entropy thresholding," *Pattern Recognit.*, vol. 26, no. 4, pp. 617–625, Apr. 1993.

[20] J. N. Kapur, P. K. Sahoo, and A. K. C. Wong, "A new method for gray-level picture thresholding using the entropy of the histogram," *Comput. Vis., Graph., Image Process.*, vol. 29, no. 3, pp. 273–285, Mar. 1985.

[21] S. Sarkar, N. Sen, A. Kundu, S. Das, and S. S. Chaudhuri, "A differential evolutionary multilevel segmentation of near infra-red images using Renyi's entropy," in *Proc. Int. Conf. Frontiers Intell. Comput., Theory Appl.*, vol. 199, no. 9, pp. 699–706, 2013.

[22] M. P. de Albuquerque, I. A. Esquef, A. R. G. Mello, and M. P. de Albuquerque, "Image thresholding using Tsallis entropy," *Pattern Recognit. Lett.*, vol. 25, no. 9, pp. 1059–1065, Jul. 2004.

[23] M. Masi, "A step beyond Tsallis and Renyi entropies," *Phys. Lett. A*, vol. 338, nos. 3–5, pp. 217–224, May 2005.

[24] F. Nie, P. Zhang, J. Li, and D. Ding, "A novel generalized entropy and its application in image thresholding," *Signal Process.*, vol. 134, pp. 23–34, May 2017.

[25] A. K. Bhandari and K. Rahul, "A context sensitive Masi entropy for multilevel image segmentation using moth swarm algorithm," *Infr. Phys. Technol.*, vol. 98, pp. 132–154, May 2019.

[26] S. Shubham and A. K. Bhandari, "A generalized Masi entropy based efficient multilevel thresholding method for color image segmentation," *Multimedia Tools Appl.*, vol. 78, no. 12, pp. 17197–17238, Jan. 2019.

[27] J. Kittler and J. Illingworth, "Minimum error thresholding," *Pattern Recognit.*, vol. 19, no. 1, pp. 41–47, Jan. 1986.

[28] S. Wang, F.-L. Chung, and F. Xiong, "A novel image thresholding method based on parzen window estimate," *Pattern Recognit.*, vol. 41, no. 1, pp. 117–129, Jan. 2008.

[29] M. H. Sulaiman, Z. Mustaffa, M. M. Saari, and H. Daniyal, "Barnacles mating optimizer: A new bio-inspired algorithm for solving engineering optimization problems," *Eng. Appl. Artif. Intell.*, vol. 87, Jan. 2020, Art. no. 103330.

[30] D. H. Wolpert and W. G. Macready, "No free lunch theorems for optimization," *IEEE Trans. Evol. Comput.*, vol. 1, no. 1, pp. 67–82, Apr. 1997.

[31] O. Q. Saber and A. Z. Yahya, "Feature selection using particle swarm optimization based logistic regression model," *Chemometrics Intell. Lab. Syst.*, vol. 182, pp. 41–46, Nov. 2018.

[32] K. Ghazvini, M. Yousefi, F. Firoozeh, and S. Mansouri, "Predictors of tuberculosis: Application of a logistic regression model," *Gene Rep.*, vol. 17, Dec. 2019, Art. no. 100527.

[33] S. Saremi, S. Mirjalili, and A. Lewis, "Biogeography-based optimisation with chaos," *Neural Comput. Appl.*, vol. 25, no. 5, pp. 1077–1097, Apr. 2014.

[34] J. A. Koupaei, S. M. M. Hosseini, and F. M. M. Ghaini, "A new optimization algorithm based on chaotic maps and golden section search method," *Eng. Appl. Artif. Intell.*, vol. 50, pp. 201–214, Apr. 2016.

[35] A. Naanaa, "Fast chaotic optimization algorithm based on spatiotemporal maps for global optimization," *Appl. Math. Comput.*, vol. 269, pp. 402–411, Oct. 2015.

[36] D. Yang, Z. Liu, and J. Zhou, "Chaos optimization algorithms based on chaotic maps with different probability distribution and search speed for global optimization," *Commun. Nonlinear Sci. Numer. Simul.*, vol. 19, no. 4, pp. 1229–1246, Apr. 2014.

[37] L.-Y. Chuang, C.-H. Yang, and J.-C. Li, "Chaotic maps based on binary particle swarm optimization for feature selection," *Appl. Soft Comput.*, vol. 11, no. 1, pp. 239–248, Jan. 2011.

[38] R. Roy and S. Laha, "Optimization of stego image retaining secret information using genetic algorithm with 8-connected PSNR," *Procedia Comput. Sci.*, vol. 60, pp. 468–477, 2015.

[39] A. Tanchenko, "Visual-PSNR measure of image quality," *J. Vis. Commun. Image Represent.*, vol. 25, no. 5, pp. 874–878, Jul. 2014.

[40] Z. Wang, A. C. Bovik, H. R. Sheikh, and E. P. Simoncelli, "Image quality assessment: From error visibility to structural similarity," *IEEE Trans. Image Process.*, vol. 13, no. 4, pp. 600–612, Apr. 2004.

[41] V. Bruni and D. Vitulano, "An entropy based approach for SSIM speed up," *Signal Process.*, vol. 135, pp. 198–209, Jun. 2017.

[42] C. Li and A. C. Bovik, "Content-partitioned structural similarity index for image quality assessment," *Signal Process., Image Commun.*, vol. 25, no. 7, pp. 517–526, Aug. 2010.
[43] L. Zhang, L. Zhang, X. Mou, and D. Zhang, "FSIM: A feature similarity index for image quality assessment," *IEEE Trans. Image Process.*, vol. 20, no. 8, pp. 2378–2386, Aug. 2011.
[44] J. John, M. S. Nair, P. R. A. Kumar, and M. Wilscy, "A novel approach for detection and delineation of cell nuclei using feature similarity index measure," *Biocybernetics Biomed. Eng.*, vol. 36, no. 1, pp. 76–88, Aug. 2016.
[45] F. Wilcoxon, "Individual comparisons by ranking methods," *Biometrics Bull.*, vol. 1, no. 6, pp. 80–83, 1945.
[46] R. S. M. D. Barros, J. I. G. Hidalgo, and D. R. D. L. Cabral, "Wilcoxon rank sum test drift detector," *Neurocomputing*, vol. 275, pp. 1954–1963, Jan. 2018.
[47] M. Friedman, "The use of ranks to avoid the assumption normality implicit in the analysis of variance," *J. Amer. Stat. Assoc.*, vol. 32, no. 200, pp. 675–701, 1937.
[48] A. K. Bhandari, A. Kumar, and G. K. Singh, "Modified artificial bee colony based computationally efficient multilevel thresholding for satellite image segmentation using Kapur's, Otsu and Tsallis functions," *Expert Syst. Appl.*, vol. 42, no. 3, pp. 1573–1601, Feb. 2015.
[49] M. H. Mozaffari, H. Abdy, and S. H. Zahiri, "IPO: An inclined planes system optimization algorithm," *Comput. Inf.*, vol. 35, no. 1, pp. 222–240, May 2016.
[50] M. H. Mozaffari and W.-S. Lee, "Convergent heterogeneous particle swarm optimisation algorithm for multilevel image thresholding segmentation," *IET Image Process.*, vol. 11, no. 8, pp. 605–619, Aug. 2017.
[51] D. Oliva, S. Hinojosa, E. Cuevas, G. Pajares, O. Avalos, and J. Gálvez, "Cross entropy based thresholding for magnetic resonance brain images using crow search algorithm," *Expert Syst. Appl.*, vol. 79, pp. 164–180, Aug. 2017.
[52] H. Liang, H. Jia, Z. Xing, J. Ma, and X. Peng, "Modified grasshopper algorithm based multilevel thresholding for color image segmentation," *IEEE Access*, vol. 7, pp. 11258–11295, Jan. 2019.
[53] S. Pare, A. Kumar, V. Bajaj, and G. K. Singh, "An efficient method for multilevel color image thresholding using cuckoo search algorithm based on minimum cross entropy," *Appl. Soft Comput.*, vol. 61, pp. 570–592, Dec. 2017.
[54] S. Kotte, P. R. Kumar, and S. K. Injeti, "An efficient approach for optimal multilevel thresholding selection for gray scale images based on improved differential search algorithm," *Ain Shams Eng. J.*, vol. 9, no. 4, pp. 1043–1067, Dec. 2018.
[55] H. S. Gill, B. S. Khehra, A. Singh, and L. Kaur, "Teaching-learning-based optimization algorithm to minimize cross entropy for selecting multilevel threshold values," *Egyptian Informat. J.*, vol. 20, no. 1, pp. 11–25, Mar. 2019.
[56] S. J. Mousavira and H. Ebrahimpour-Komleh, "Human mental search based multilevel thresholding for image segmentation," *Appl. Soft Comput.*, Apr. 2019, Art. no. 105427, doi: 10.1016/j.asoc.2019.04.002.
[57] V. K. Bohat and K. V. Arya, "A new heuristic for multilevel thresholding of images," *Expert Syst. Appl.*, vol. 117, pp. 176–203, Mar. 2019.
[58] A. K. Bhandari, "A novel beta differential evolution algorithm-based fast multilevel thresholding for color image segmentation," *Neural Comput. Appl.*, vol. 32, no. 9, pp. 4583–4613, Oct. 2018.
[59] M. A. Elaziz, A. A. Ewees, D. Yousri, D. Oliva, S. Lu, and E. Cuevas, "A competitive swarm algorithm for image segmentation guided by opposite fuzzy entropy," in *Proc. IEEE Int. Conf. Fuzzy Syst. (FUZZ-IEEE)*, Glasgow, U.K., Jul. 2020, pp. 1–8.
[60] S. J. Mousavirad, G. Schaefer, and H. Ebrahimpour-Komleh, "A benchmark of population-based metaheuristic algorithms for high-dimensional multi-level image thresholding," in *Proc. IEEE Congr. Evol. Comput. (CEC)*, Wellington, New Zealand, Jun. 2019, pp. 2394–2401.
[61] D. Oliva, M. S. R. Martins, V. Osuna-Enciso, and E. F. de Morais, "Combining information from thresholding techniques through an evolutionary Bayesian network algorithm," *Appl. Soft Comput.*, vol. 90, May 2020, Art. no. 106147.
[62] E. Rodríguez-Esparza, L. A. Zanella-Calzada, D. Oliva, A. A. Heidari, D. Zaldivar, M. Pérez-Cisneros, and L. K. Foong, "An efficient harris hawks-inspired image segmentation method," *Expert Syst. Appl.*, vol. 155, Oct. 2020, Art. no. 113428.
[63] V. Rajinikanth and M. S. Couceiro, "RGB histogram based color image segmentation using firefly algorithm," *Procedia Comput. Sci.*, vol. 46, pp. 1449–1457, 2015.
[64] F. Chakraborty, D. Nandi, and P. K. Roy, "Oppositional symbiotic organisms search optimization for multilevel thresholding of color image," *Appl. Soft Comput.*, vol. 82, Sep. 2019, Art. no. 105577.
[65] H. Jia, X. Peng, W. Song, D. Oliva, C. Lang, and Y. Li, "Masi entropy for satellite color image segmentation using tournament-based Lévy multiverse optimization algorithm," *Remote Sens.*, vol. 11, no. 8, p. 942, Apr. 2019.
[66] M. Barazandeh, C. S. Davis, C. J. Neufeld, D. W. Coltman, and A. R. Palmer, "Something Darwin didn't know about barnacles: Spermcast mating in a common stalked species," *Proc. Roy. Soc. B, Biol. Sci.*, vol. 280, no. 1754, Mar. 2013, Art. no. 20122919.
[67] J. F. Crow, "Hardy, Weinberg and language impediments," *Genetics*, vol. 152, no. 3, pp. 821–825, Aug. 1999.
[68] S. W. Guo and E. A. Thompson, "Performing the exact test of Hardy Weinberg proportion for multiple alleles," *Biometrics*, vol. 48, no. 2, pp. 361–372, 1992.
[69] G. Brusca and R. Brusca. (2002). *Figure of Barnacles Adopted From WWW Document*. [Online]. Available: http://www.uas.alaska.edu/arts_sciences/naturalsciences/biology/tamone/catalog/arthropoda/balanus_glandula/reproduction_and_development.html
[70] W. H. David, L. Stanley, and X. S. Rodney, "Introduction to the logistic regression model," in *Applied Logistic Regression*, vol. 1, 3rd ed., A. S. Walter, Ed. New York, NY, USA: Wiley, 2013, pp. 1–33.
[71] A. H. Gandomi and A. H. Alavi, "Krill herd: A new bio-inspired optimization algorithm," *Commun. Nonlinear Sci. Numer. Simul.*, vol. 17, no. 12, pp. 4831–4845, Dec. 2012.
[72] A. H. Gandomi, X.-S. Yang, S. Talatahari, and A. H. Alavi, "Firefly algorithm with chaos," *Commun. Nonlinear Sci. Numer. Simul.*, vol. 18, no. 1, pp. 89–98, Jan. 2013.
[73] N. Wang, L. Liu, and L. Liu, "Genetic algorithm in chaos," *Oper. Res. Trans.*, vol. 5, pp. 1–10, Jan. 2001.
[74] V. Jothiprakash and R. Arunkumar, "Optimization of hydropower reservoir using evolutionary algorithms coupled with chaos," *Water Resour. Manage.*, vol. 27, no. 7, pp. 1963–1979, Jan. 2013.
[75] Z. Guo, B. Cheng, M. Ye, and B. Cao, "Self-adaptive chaos differential evolution," *Adv. Natural Comput.*, vol. 4221, pp. 972–975, Sep. 2006.
[76] D. Simon, "Biogeography-based optimization," *IEEE Trans. Evol. Comput.*, vol. 12, no. 6, pp. 702–713, Mar. 2008.
[77] D. Du, D. Simon, and M. Ergezer, "Biogeography-based optimization combined with evolutionary strategy and immigration refusal," in *Proc. IEEE Int. Conf. Syst., Man Cybern.*, San Antonio, TX, USA, Oct. 2009, pp. 997–1002.
[78] A. Bhattacharya and P. K. Chattopadhyay, "Hybrid differential evolution with biogeography-based optimization for solution of economic load dispatch," *IEEE Trans. Power Syst.*, vol. 25, no. 4, pp. 1955–1964, Nov. 2010.
[79] A. Faramarzi, M. Heidarinejad, B. Stephens, and S. Mirjalili, "Equilibrium optimizer: A novel optimization algorithm," *Knowl.-Based Syst.*, vol. 191, Mar. 2020, Art. no. 105190.
[80] A. Faramarzi, M. Heidarinejad, S. Mirjalili, and A. H. Gandomi, "Marine predators algorithm: A nature-inspired metaheuristic," *Expert Syst. Appl.*, vol. 152, Aug. 2020, Art. no. 113377.
[81] *Landsat Imagery Courtesy of NASA Goddard Space Flight Center and U.S. Geological Survey*. Accessed: Jul. 6, 2020. [Online]. Available: https://landsat.visibleearth.nasa.gov/index.php?&p=1

HONGBO LI was born in Harbin, China, in 1990. He received the B.S. degree from the College of Mechanical and Electrical Engineering, Hainan University, Haikou, China, in 2013, and the M.S. degree from the College of Mechanical and Electrical Engineering, Northeast Forestry University, Harbin, in 2016, where he is currently pursuing the Ph.D. degree in forestry engineering automation. His research interests include machine learning, image segmentation, and metaheuristic algorithm.

GANG ZHENG received the M.S. degree in agricultural electrification and automation from Northeast Forestry University, China, in 2008. He is currently a Lecturer with Northeast Forestry University. His research interests include intelligent detection, information fusion, and image processing.

KANGJIAN SUN was born in Jinzhou, China, in 1996. He received the B.E. degree in electrical engineering and automation from Northeast Forestry University, Harbin, China, in 2019, where he is currently pursuing the M.E. degree in control engineering from the College of Mechanical and Electrical Engineering. His research interests include swarm optimization algorithm, image segmentation, and feature selection.

ZICHAO JIANG was born in Qiqihar, China, in 1995. He is currently pursuing the M.S. degree in control theory and control engineering from Northeast Forestry University, China. His research interests include image segmentation and swarm intelligence algorithm.

YAO LI was born in Yichun, China, in 1997. She is currently pursuing the M.S. degree in control theory and control engineering from Northeast Forestry University, China. Her research interests include image segmentation and swarm intelligence optimization.

HEMING JIA (Member, IEEE) received the Ph.D. degree in system engineering from Harbin Engineering University, China, in 2012. He is currently a Professor with Sanming University. His research interests include nonlinear control theory and application, image segmentation, and swarm optimization algorithm.